Investigations of the Neural Firing Threshold

Carsten Erdmann

September 2011

Im Fachbereich Biologie, Chemie, Pharmazie der Freien Universität Berlin
eingereichte Dissertation

1. Gutachter: Prof. R. Menzel, Freie Universität Berlin

2. Gutachter: Prof. U. Heinemann, Charité Berlin

Tag der Prüfung: 17.4.2012

Hiermit versichere ich, die vorliegende Dissertation selbstständig angefertigt und keine außer den angegebenen Hilfsmitteln verwendet zu haben.

Ottersberg, 30.9.2011 .....

(Carsten Erdmann)

Auch die längste Reise beginnt mit einem Schritt.

Chinese saying

Papa, das geht doch nicht, dass Du jedes Wochenende das ganze Wochenende nur an Deiner blöden Arbeit schreibst!

Lena Erdmann

Contents

List of Figures

Nomenclature

2D Two-dimensional

3D Three-dimensional

4-AP 4-Aminopyridine

ACSF Artificial cereospinal fluid

AMPA Alpha-amino-3-hydroxy-5-methyl-4-isoxazolepropionic acid

AP Action Potential

APV (2R)-amino-5-phosphonovaleric acid, a selective NMDA receptor antagonist

CA cornu ammonis, a curved structure of densly packed neuronal somata within the hippocampal formation

CGP-55845A [(2S)-3-[[(1S)-1-(3,4-dichlorophenyl)ethyl]amino]-2-hydroxypropyl] (phenylmethyl) phosphinic acid, a $GABA_B$ antagonist

CNQX 6-cyano-7-nitroquinoxaline-2,3-dione, a competitive AMPA/Kainate receptor antagonist

DG dentate gyrus, a V-formed structure of neuronal somata within the hippocampus

fSIP found SIP: SIP found by using the forward/backward regression Method

GABA Gamma-aminobutyric acid

LIF leaky integrate-and-fire

NMDA N-Methyl-D-Aspartat

PCI Peripheral Component Interconnect, a computer bus for attaching hardware devices to a computer

rSIP real SIP: SIP determined by shortening the stimulus until no spike appeared.

SEM Standard error of mean

SIP spike initiation point, the point of no return within the cell's voltage trace. If the signal exceeds this point a spike is unavoidable.

U Voltage, here the membrane voltage

$\dot{U}$ first time derivative of the voltage

Chapter 1

Introduction

Concerning the brain's information processing capabilities, neurons are the central elements of brain function. They communicate via action potentials (APs, also called spikes) sent to each other along the axons and transmitted through synapses.

Despite the fact that more and more detailed knowledge erode many neurobiological dogmata it seems still generally correct to stick to the views that dendrite and soma are the input and processing regions for incoming signals, that the action potentials are generated from the membrane potential fluctuations somewhere around the axon hillock, that spikes are the binary elements of the neural language, and that they are transmitted along the axon.

Looking at the spikes as the key element of neural language, and focusing at the widely recorded intracellular membrane potential, this work will focus on the central question: what are the voltage conditions within a neural soma that elicit a spike? It is generally agreed that spikes are generated by a voltage threshold within the neuron, i.e. there is one fixed threshold level the exceedance of which elicits a spike. However, it is also long known that the voltage threshold may vary in central neurons (e.g. see [44, 9, 5] and also [36]) as well as in distant elements such as the neuromuscular junction (e.g. see [38]).

When looking at the spike generator from the viewpoint of dynamical systems mathematics, the variable U for the voltage would thus be its state variable, and the associated state space would then be one-dimensional. But the fact that the threshold varies within the neuron immediately indicates that the state space is too low-dimensional and demands the introduction of further state variables.

1.1 Approach

The threshold concept of spike initiation has first been thoroughly described by the work of Bernstein in 1871 and 1902 ([6, 7]), but has been around for quite some time before (see [30] for a short overview). It has of course proven to be both simple and useful. However, short after Bernsteins work Lucas ([30]) relativised the threshold concept by reporting its variability. Since then it has often been reported qualitatively that a neuron, although firing at its (voltage) threshold, may be driven far above this threshold by sufficiently shallow depolarizing ramps without eliciting a spike. It has also been shown that the voltage threshold depends on stimulus form (e.g. see [5]). The connecting feature between these findings is the slope of the internal voltage changes, i.e. the first time derivative, $\frac{dU}{dt}$ or $\dot{U}$, of the voltage. Bryant and Segundo proposed 1976 [10] that the stimulus slope is a relevant parameter for spike initiation, however this did not result in an extension of the neural state space. These considerations lead us to the idea to investigate $\dot{U}$ as a possible second state variable for the neural spike generator.

We will address this hypothesis by stimulating cells in vitro and in silico with current ramps of different slope. However, with this approach we will not be able to directly control the membrane potential as active processes and nonlinear elements in the membrane will affect the effective slope of the membrane potential change. Using a voltage clamp setup, one could control the voltage slope, but this would both eliminate the effects of natural active/nonlinear processes as well as possibly impede precise locating the spike start in its original form.

The soma is the most likely area to hit with a recording electrode, especially in a "blind" setup as will be used here. A central assumption now is that the spike generator is located inside the range of a sufficiently good space clamp with the soma. There are papers showing that the point of spike initiation varies in one cell (e.g see [34]), or that it lies quite far down in the axon (e.g. see [46]). In these cases one would have to doubt the quality of the space clamp. However, there are no means by which this could be ruled out with this experimental design. We do see our approach to be nevertheless useful as it aims at developing a pragmatic and phenomenological tool for data analysis of intracellular data.

After recording the cell's reaction to the stimulus we will use a novel algorithm to precisely detect the "point of no return" in spike initiation, the spike initiation point (SIP) on the voltage trace, thus being able to determine both U as well as $\dot{U}$ at this exact point. With these data at hand, we can then analyze the neural spike generator within its new two-dimensional state space projection, checking the validity of $\dot{U}$ as a second state variable.

For this task we will have to solve two central problems:

1. In order to determine the precise point at which the spike emerges from the pre-spike dynamic we will have to focus on this exact region. In order to investigate U and $\dot{U}$ there we will have to invent an algorithm that is capable of determining the SIP for each spike with high resolution and precision. With these SIPs at hand we will be able to determine both U and $\dot{U}$ for each SIP, thus allowing the second analytic step.

2. We will then run experiments on cells and models. In order to verify the concept of a two-dimensional state space we will simulate them with ramps of different slopes, thus inducing various voltage slopes at the points of spike initiation. After detecting the SIPs of these spikes we can then analyze the relevance of $\dot{U}$ as a second state variable.

1.2 Concepts

1.2.1 2-Dimensional State Space

With the intention to extend the state space to two dimensions, we will have to do all further analysis within this new state space. This new way of looking at a spike has been introduced in former work ([18]) and is currently more and more used to look at spike properties. It is a combination of the two state variables U and $\dot{U}$ (see figure 1.1).

This view also shows another interesting fact. Here we are able to distinguish two different types of system dynamics:

1. in the left part of the state space we find the small circular wiggles of passive sub-threshold dynamics due to some synaptic input or noise

2. in the right part we see the active spike dynamics which reminds of a big circle

These two types of dynamics are clearly segregated and show very different properties. This gives rise to the hope that we could somehow be able to distinguish both types of dynamics.

1.2.2 The Spike Initiation Point (SIP)

The SIP will be exactly the point at which the wiggling pre-spike dynamic switches to the circular spike dynamic. It can thus be defined by the following features:

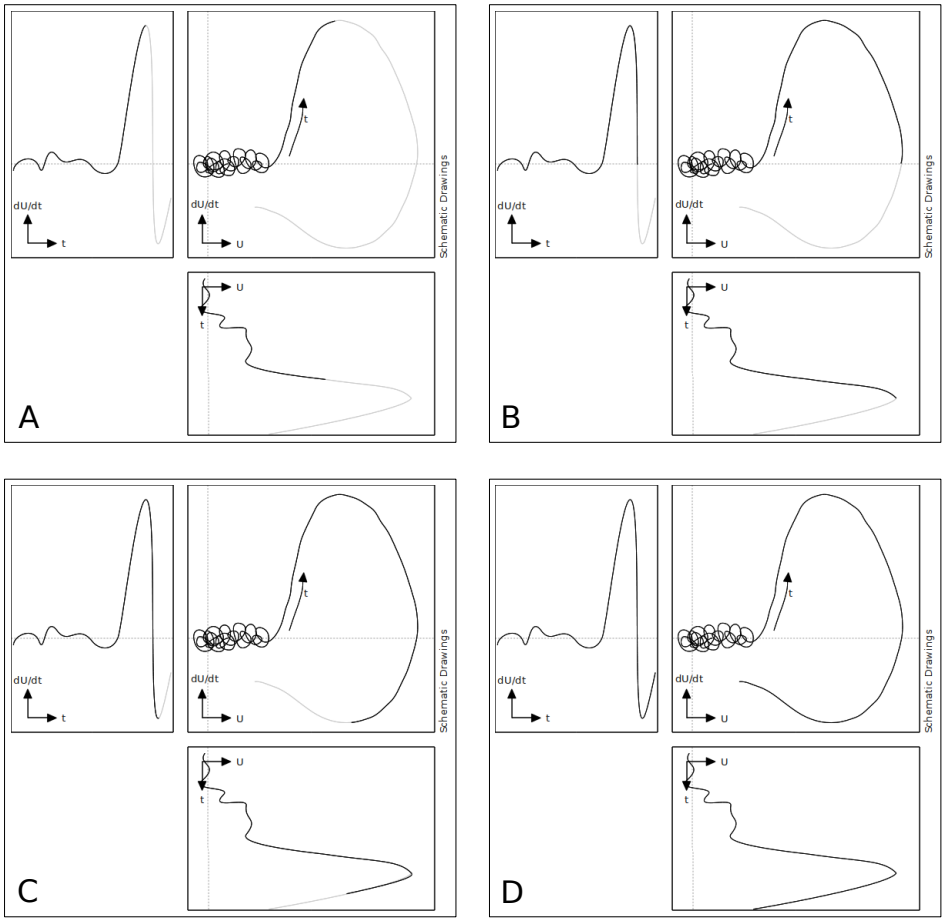

Figure 1.1: Construction of a spike in the 2-dimensional state space.
Each sub picture A, B, C, D consists of an $\dot{U}$ against time plot (left), an U against time plot (bottom), and the state space as a combination of those two ($\dot{U}$ against U, big plot). Note that there is no time axis in the state space plot, here the time runs along the trajectory. The gray curve shows the complete signal, whereas the black curve shows 4 different time steps during construction of the state space trajectory. The wiggle before the spike resembles the pre-spike sub-threshold membrane potential fluctuations. The sub pictures show 4 central elements of the spike. A: $\dot{U}$ maximum (i.e. steepest part of voltage spike upstroke), B: U maximum at $\dot{U} = 0$ (voltage maximum), C: $\dot{U}$ minimum (steepest part of voltage spike downstroke), and finally D: the complete spike.
All figures shown are schematic drawings.

- It is the point of no return: once crossed, the system will unavoidably run into a spike, even if the stimulus is switched off exactly at the SIP.
- It is the point at which the trajectory changes its typical pre-spike behavior (small circles), gains speed and abruptly runs into the big spike circle

We will not be able to investigate the first feature in real cells as this would mean to switch off the stimulus abruptly at the SIP. This would induce strong artifacts, distorting the voltage trace and thus making the delicate SIP analysis impossible. However, we will be able to run this kind of experiments with models.

1.2.3 The Threshold Separatrix

In the analysis of dynamical systems situations are often similar to the problem we encounter here. Within a given state space there may be certain attractors or repellers, influencing the course of the trajectory in dependence of its starting condition. Between two given attractors there is a discrete borderline: If the system starts on one side of this border, it will unavoidably run into the one attractor, and it will run into the other one if started on the other side. Such a line is called a separatrix.

There is only one simple attractor within our system: the resting potential. If the system is distorted by some subthreshold value it will unavoidably return to the resting potential. The spike is not a real second attractor because the system will - after running through a spike - return to the resting potential instead of staying in the spike. However, focusing on the point of spike initiation it is justifiable to imagine the spike dynamic - namely the Na equilibrium potential - to be a second attractor. Doing so, it seems reasonable and useful to adopt the concept of a separatrix for the spike generator as a possible threshold definition within the 2D state space.

Because the SIPs are defined as the irreversible transition points to the spike dynamic, this concept would mean that the separatrix is the curve defined by all SIPs of the cell. It will thus be a hyperplane within the state space. In order to determine it, it is necessary to precisely define the SIP within each spike trajectory.

4-Aminopyridine is long known to be a classical inhibitor especially for the A-type potassium channels. The currents mediated by these channels are transient potassium currents activating at -50 mV. As they influence the firing threshold (e.g. see [20, 27]), our idea was to investigate the possible role of the A-type potassium current on the spike threshold: whether it would shift, distort or switch separatrices.

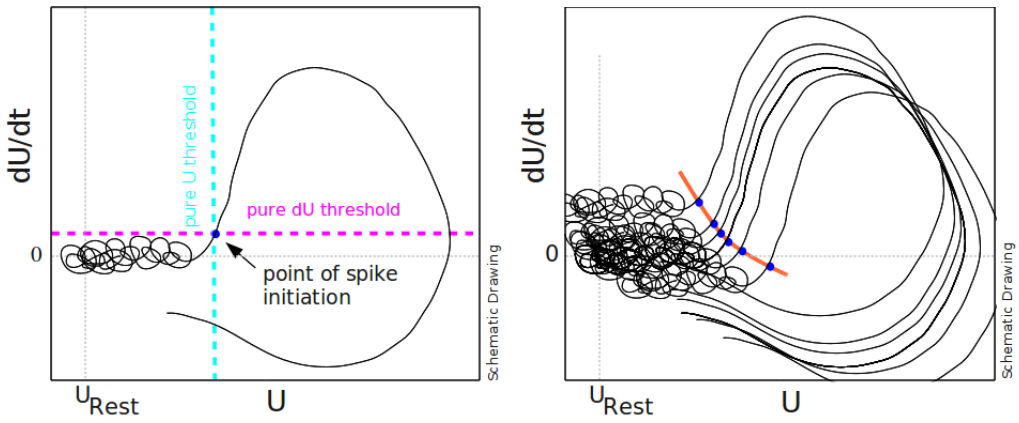

Figure 1.2: The SIP and separatrix concepts.
Both figures show schematic drawings of spikes in the $U - \dot{U}$ state space. Left: The SIP ("point of spike initiation") marks the unavoidable transition into the spike dynamic. In the state space plot the classic voltage threshold would be resembled by the blue dashed line: all SIPs would lie vertically aligned at the same voltage value. In case of a $\dot{U}$ threshold it would be a vertical line (magenta), with all spikes starting at the same slope but at different voltages. Right: Blue dots denote SIPs of the spikes displayed. The separatrix (orange) is then the line formed by connecting all SIPs of one cell.

1.3 Questions to the System

Based on these considerations, we will try to answer these questions:

- How can we precisely determine the SIP for a spike?
- Is $\dot{U}$ a suitable second threshold parameter?
  - Do cells and models exhibit separatrices?
  - Is a 2-D state space sufficient?
  - How do separatrices look like?
  - Do model separatrices differ from biological ones?
  - Does a block of the A-type potassium channels affect the separatrices?

Chapter 2

A new Algorithm for Precise Detection of the Point of Spike Initiation

2.1 Materials and Methods

The analysis procedures described here were performed on voltage data of action potentials, their time derivative as well as the appropriate stimulus signals. All signals were sampled with 35 kHz. They were recorded *in vivo* and simulated *in silico* according to the methods described in section 3.1. Please refer to that section for details on materials, recording, modeling or the like.

2.1.1 Finding the SIP

As has been stated above (see 1.2.1), the SIP defines the transition from the passive pre-spike (i.e. sub-threshold) dynamic to the active (i.e. super-threshold) spike dynamic. The algorithm presented here will make use of the distinct features of the two types of dynamic in the U-$\dot{U}$-plane.

To find the transition point, we will try to estimate it from within the pre-spike regime as well as from within the spike regime (see fig. 2.1). Within the pre-spike dynamic, we take a 2.8 ms (100 data points at 35 kHz) long data window which is near the spike, but still clearly inside the passive regime. This is assured by defining a fixed distance of 0.6 ms (20 data points at 35 kHz) from the spike's voltage maximum which is easy to detect. We calculate a linear regression from these data, thus projecting its trace beyond the SIP. This is justifiable as the pre-spike dynamics is slow in relation to the

Algorithm 2.1 Algorithm for the SIP finder

```
START
# finding the SIPs from a voltage trace
Find spike maxima
Convert voltage data to 2-D U-dU data
Define data window relative to max(U) directly before, but clearly not inside spike
Determine suitable extrapolation function through these data
Define data window left of max(dU) spanning about 1/8 of the spike circle
Determine linear regression function through these data
For (each spike max)
  determine intersection between linear regression functions
  While (SIP not found)
    move spike window one data point backward
    determine actual intersection between linear regression functions
    If (actual intersection is right of last intersection)
      last intersection = actual intersection
    Else
      identify data point nearest to last intersection point
      SIP = identified nearest data point
    Endif
  Endwhile
  Append SIP to SIP-List
Endfor
Return SIP-List
STOP
```

short data window as well as in comparison to the spike dynamic, especially for the simple ramp stimuli used in this study.

Within the spike regime, we start at $\max(\dot{U})$ and define a similar window left from there with a length of 0.14 ms (4 data points at 35 kHz). We calculate the linear regression from this window as well and use it as a backward estimate for the spike dynamic. As the spike trace is nearly linear at spike start, this turns out to be a suitable assumption[1]. As an estimate for the SIP, we then calculate the intersection point of both regression lines which will lie far left at this first step. In each subsequent iteration, the in-spike regression window is shifted left (i.e. backward in time) one data point at each step while the window size is kept constant. As a consequence, the in-spike regression line will become steeper and steeper, and the intersection point will shift right on the pre-spike regression line with each iteration. With the in-spike data window moving backward in time, it will eventually enter the pre-spike regime, thus resulting in a shallower regression line and thus in the intersection point shifting left again. The algorithm stops here, returning the rightmost intersection point as the best estimate for the SIP. This estimate is then mapped to the real data by choosing the data point with the smallest euclidean distance to the SIP estimate.

[1] More sophisticated fits have also been tested, but they turned out to be too prone to slight variations in spike onset dynamics.

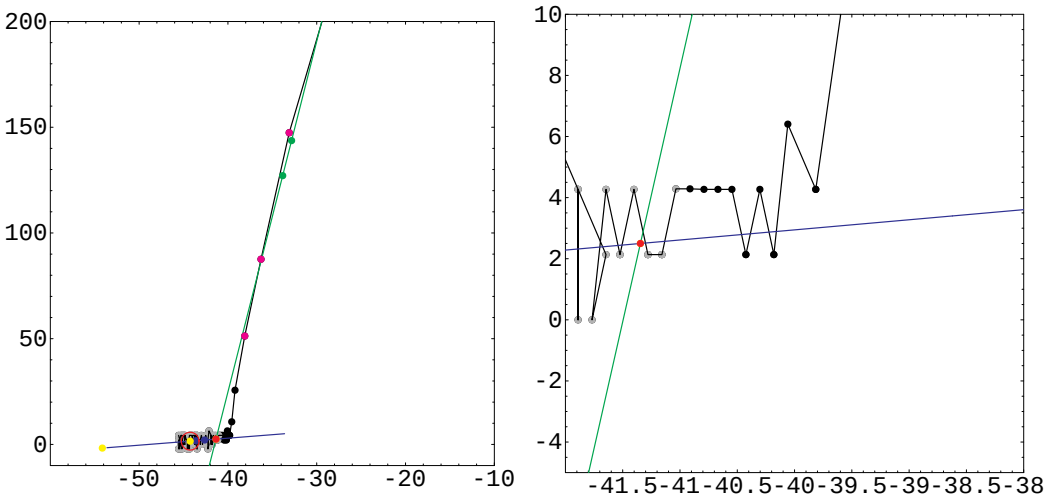

Figure 2.1: SIP Finder: first snapshot.
This figure illustrates an early stage of the SIP finder process (see figures 2.2 and 2.3 for subsequent snapshots). Within all 3 figures the left plot displays the spike onset in the state space, with the dense dots resembling the passive pre-spike dynamics followed by the start of the (active) spike trajectory. The right plot in each figure shows a magnified view of the transition point. The gray points are the data clearly within the pre-spike dynamic which are used to calculate the linear pre-spike regression (blue line, blue dots are the calculated supporting points). The magenta-colored points are clearly within the spike dynamic, their linear regression is the green line (green dots are the calculated supporting points). The red dot is the current intersection of both regression lines, the yellow dots resemble the previous intersection points. The red circle denotes the previous intersection point relative to the current one.
U [mV] is on horizontal axis, $\dot{U}$ [mV/ms] at vertical axis.

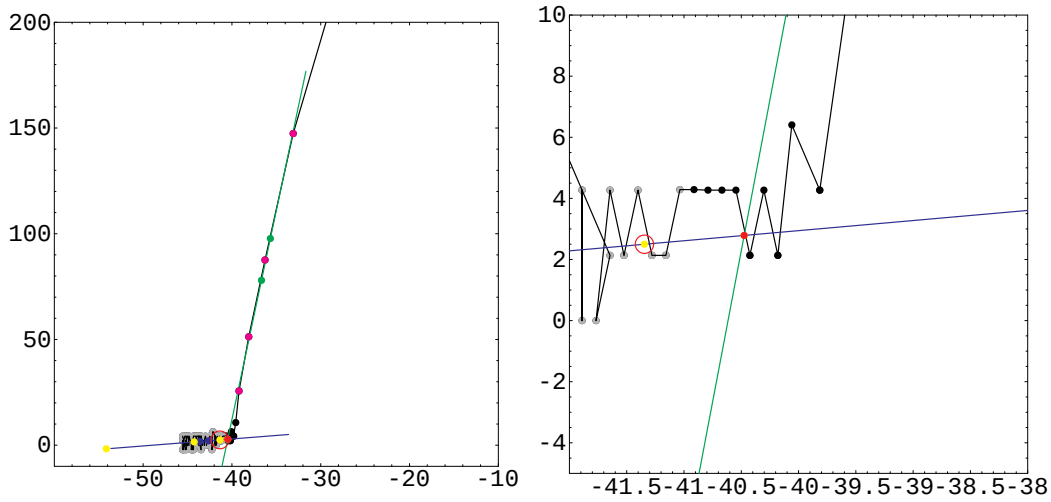

Figure 2.2: SIP Finder: second snapshot.
This figure shows the next step after figure 2.1. The in-spike regression window has been shifted backward in time by one data point. The resulting green regression line intersects with the blue pre-spike line more right than before (see red dot). The previous intersection point (red dot in left figure2.1) is now yellow, marked with a red circle. With each step the intersection point shifts more and more right on the blue pre-spike regression line. See figure 2.1 for figure legend.

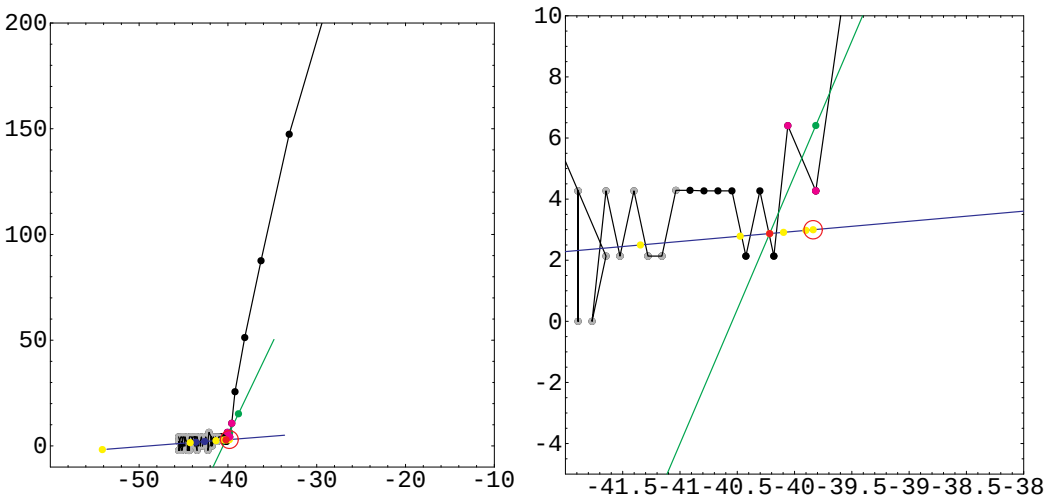

Figure 2.3: SIP Finder: final snapshot.
This figure illustrates the final stage of the SIP finder sequence. The right figure is the last step in the process: now the left boundary of the in-spike regression window has reached the pre spike dynamic, resulting in a shallower green regression line. This causes the regression intersection to be more left on the blue regression line (compare red dot with red circle denoting the last intersection point. This causes the process to stop, and the rightmost intersection point is taken to be the first estimate for the SIP. See figure 2.1 for figure legend.

2.1.2 Checking the SIP finder

In order to verify the precise function of the SIP finder we need an alternative way to determine the transition point from pre-spike to spike dynamic. As this point is defined as the point-of-no-return we can find it by making the stimulus ramp shorter and shorter until no spike is elicited any more. This would thus mean to switch off the stimulus exactly at the SIP. Despite all efforts for a clean adjustment of electrode and recording parameters artifacts in the recorded voltage trace (due to the sharp edge at stimulus switch-off) could not be avoided. As the delicate analysis of the SIPs would have been thoroughly affected by these artifacts this procedure was carried out solely on models.

In this approach the SIP is searched for using the binary search algorithm. The iterative procedure starts with a ramp stimulus of an initial length L_0. In the next steps the ramp is either elongated (if the last iteration did not elicit a spike) to $L_{n+1} = L_n + \frac{L_n}{2}$ or shortened (if the last iteration did elicit a spike) to $L_{n+1} = L_n - \frac{L_n}{2}$ for iteration n with $n = 0$ at the initial step. This is repeated until a temporal resolution of $\Delta t \leqq 0.001$ ms is reached.

These real SIPs (rSIPs) can then be compared to the finder's SIPs (fSIPs) by calculating the temporal difference between both points. Using the separatrix concept presented in chapter 3 we can also analyze the temporal distance between complete separatrices.

2.2 Results

2.2.1 SIP Finder

For all natural spikes analyzed we can precisely and robustly determine the phenomenological SIP with the algorithm described here. "Precisely" means that the fSIPs - the only ones available for natural spikes - are both plausible in U and $\dot{U}$ as well as very close to the pre-spike subthreshold dynamic (see fig. 2.4). "Robustly" means that the SIP finder is able to find the SIP in all cases of healthy spikes.

With the stimulus shortening procedure using the simulated models we have an alternative tool at hand (see 2.1.2) to determine the real SIPs. Comparing these with the found SIPs, we encounter large differences between rSIPs and fSIPs (up to 1.3 ms) with most Hodgkin-Huxley type models used here. This means that reaching the rSIP does induce the irreversible dynamic that will lead to a spike, but obviously in the beginning this dynamic is much too weak to result in any detectable effects in the membrane voltage.

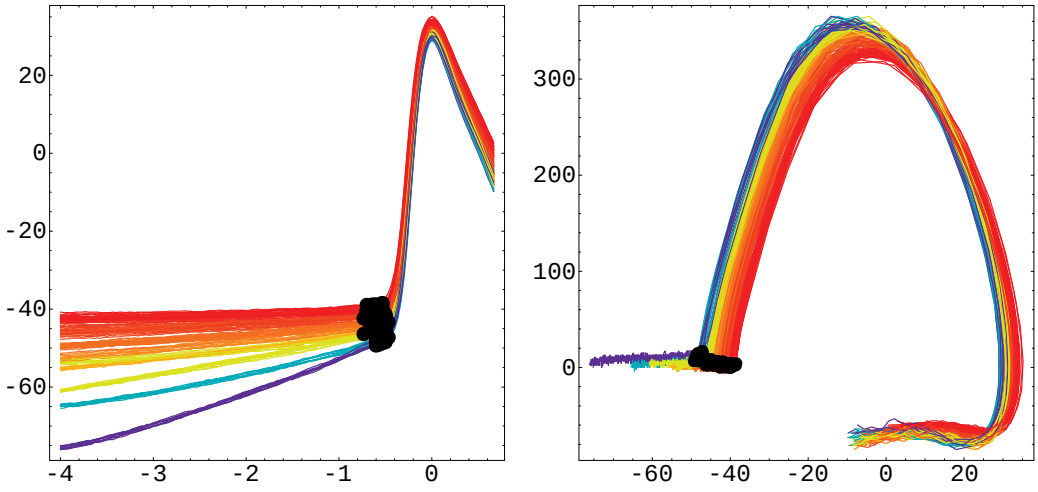

Figure 2.4: Found SIPs are plausible.
SIP location is plausible in U (left plot), $\dot{U}$ as well as in the $U/\dot{U}$ state space (right plot). Colors code from red via orange, yellow, green to blue for steepness of stimulation ramp: red means shallow ramps, blue are steep ramps. Black dots indicate position of detected SIPs.
Left plot shows voltage [mV] against time [ms], spikes are aligned with their voltage maximum at t=0. Same group of spikes is shown in right plot in state space with$U$ [mV] on the horizontal axis and $\dot{U}$ [mV/ms] on the vertical axis.

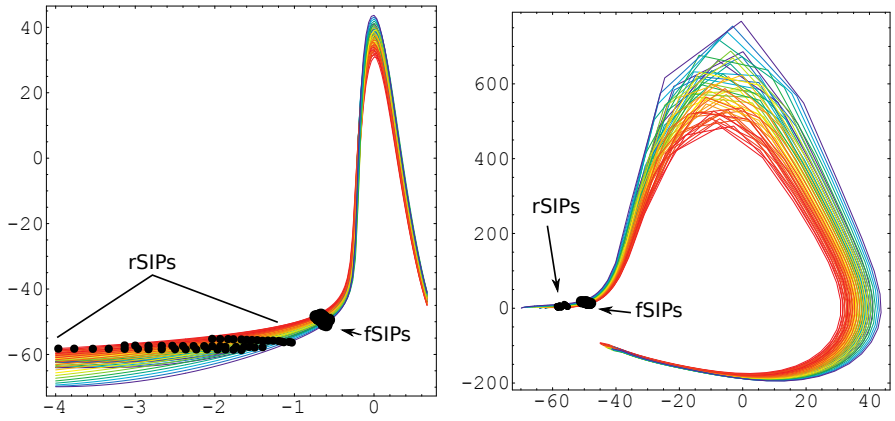

Figure 2.5: Differences of rSIPs to fSIPs in models.
This Plot shows the Wang/Buzsáki variation of the Hodgkin/Huxley type model, answering to ramp stimulation. Colors code from red via orange, yellow, green to blue for steepness of stimulation ramp: red means shallow ramps, blue are steep ramps. Black dots indicate position of detected SIPs: while the right-hand cloud of SIPs indicate the fSIPs in both plots, the left-hand cloud in the right plot as well as correspondingly the left-hand stripes of dots in the left plot show the rSIPs.
Left plot shows voltage [mV] over time [ms], spikes are aligned with their voltage maximum at t=0. Same group of spikes is shown in right plot in state space. U [mV] is on horizontal axis, $\dot{U}$ [mV/ms] at vertical axis.

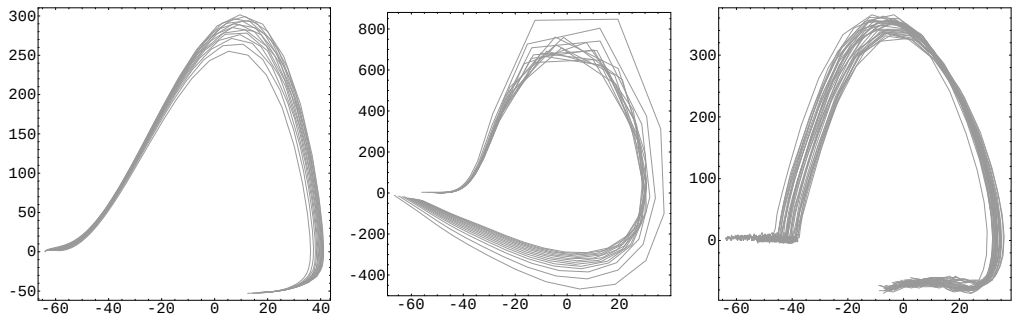

Figure 2.6: Spike dynamics in neurons and models.
Left: Trajectories of the original Hodgkin-Huxley model. Spike onset is very shallow. Middle: Trajectories of the modified Awiszus model. Note that spike onset dynamic is much faster here. Right: Trajectories of a real neuron. Spikes are still faster at spike onset, the trajectories emerge nearly vertical from the pre-spike dynamic.
See figure 2.5 for the effects of kinkiness on real and found SIPs.

Luckily, we see an interesting effect among the models. Contrary to the other Hodgkin-Huxley models tested, the modified Awiszus model does detect the fSIPs much close to the rSIPs (see fig. 3.10). This model phenomenologically differs from the other ones in so far as its spike dynamic shows a much more abrupt onset.

Close inspection of the trajectories of models and neurons reveal significant differences concerning the speed of the dynamic at spike onset (see fig. 2.6). We can see that the faster the spike dynamic at spike onset, the closer the fSIPs are to the rSIPs. As the modified Awiszus model has a much faster dynamic than the original Hodgkin-Huxley model, it allows the detection of the fSIPs much closer to the rSIPs.

Comparing the trajectories of a real neuron to those of the models, we see that it is still much faster at spike onset than any of the Hodgkin-Huxley type models. This justifies the interpretation that the fSIPs found on the neuron's trajectories are similar to the rSIPs we cannot precisely detect.

2.2.2 Late Spike Phenomenon

During the shortening of the stimulus ramps we encountered an interesting phenomenon in all Hodgkin-Huxley type models. When the ramp was shortened to determine the precise rSIP, it occurred for certain slope/duration combinations that a spike occurred far (up to 60 ms) after the stimulus had been switched off.

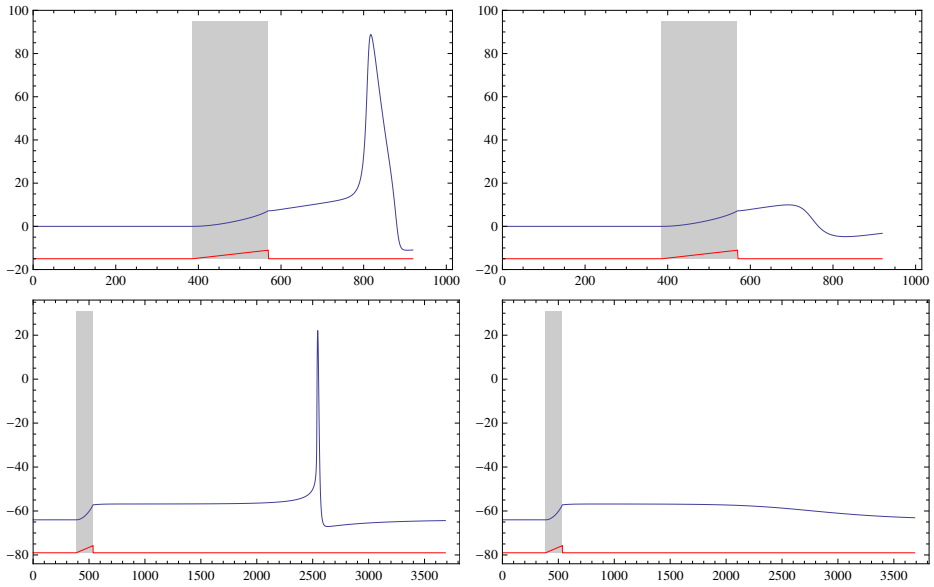

Figure 2.7: Late spike phenomenon.
Top left: a ramp of length 5.23438 ms and slope 758 mV/ms in the classic Hodgkin-Huxley model induces a spike which occurs far after the ramp has been switched off. This illustrates the concept of a "point of no return" as a definition of the SIP. Top right: a slightly shorter Ramp (5.2334 ms) does not produce a spike but only a bump instead.
The late spike phenomenon depends on the parameter set of the respective model. The lower two figures show a much longer time delay for the Wang/Buzsáki variation of the Hodgkin/Huxley type model. Ramp parameters are: Length 4.29688 ms and slope 758 mV/ms (lower left), length 4.2959 ms with the same slope (lower right). All figures: red curve shows stimulus without scale for timing information only. Grey rectangle maps beginning and end of stimulus to the voltage trace.

For our search of the rSIP this phenomenon has been taken into account by elongating the observation window after the stimulus in order not to miss such a late spike. It does not, however, interfere with our analysis as we are only interested at the SIP at this point, regardless of how long it takes for the spike to occur.

2.3 Discussion

We have presented a new algorithm that allows a precise phenomenological determination of the SIP in intracellular voltage data of neurons and certain models. It allows a new approach for the study of the spike initiation processes.

Previously, any analysis concerning the spike threshold had to define the threshold point at each spike pragmatically somewhere as low as possible, typically by applying a threshold line at the maximum value found in each inter-spike interval. This is a reasonable approach when a simple voltage threshold model is applied. If however one follows the arguments stated in chapter 1, resulting in the view of a missing state variable, one will surely miss certain features of the SIPs found using this method.

By applying the method presented here, one has a much more plausible tool to find the SIPs with high (phenomenological) precision. This may open new vistas for spike initiation research, spike timing issues or the like.

2.3.1 Point of Spike Initiation

It has been - and still is - a long discussion on where in the neuron the spike is generated. Despite the classical view that the spike is initiated at the axon hillock there have been theoretical and experimental ([16, 21, 40, 31, 32, 34, 42, 46]) approaches to answer this question, locating the spike initiation site somewhere between the soma or even far inside the axon. Because the electrical properties of these sites differ, and because the electrical properties will surely influence both stimulus form and cell response, the site of spike initiation may challenge the algorithm presented here.

As the soma is the biggest part of the neuron, it is most likely that sharp intracellular electrodes will penetrate the neuron at or at least near it, especially as many recordings are done without detailed microscopic control. If the spike is generated far from the axon it surely has to be questioned whether the detailed analysis done by the SIP finder leads to reliable SIPs.

However, the central idea behind this approach is a purely phenomenological and pragmatical one. The somatic voltage trace is what is available for a

significant amount of intracellular recordings. Thus, our aim was to create a tool that allows much more detailed analysis of threshold- and timing-related questions than it was possible up to now. Despite the unresolved question for the spike initiation site we see it justified to apply the new SIP finding algorithm presented here to recordings with a fast and abrupt dynamic at spike onset.

In the analysis presented here we have used a linear regression as the forward estimate of the pre-spike domain. This is suitable in our case where the membrane potential rises quasi linear due to the smooth stimulus ramp and the absence of any preceding spikes. When applying this analysis to real-world data with natural input and shorter interspike intervals, this approach surely will have to be verified. It may seem suitable to use a higher order polynomial as a better fit to the data in those cases.

2.3.2 Speed of Spike Dynamics

Currently an exciting discussion takes place concerning the amount as to which Hodgkin-Huxley type models are able to model relevant details of spike initiation [36, 37, 33, 22]. Naundorf et al. [36] have reported the finding that Hodgkin-Huxley type models show a much slower spike onset dynamic than real neurons as well as a high threshold variability.

Our study supports the findings of Naundorf et al. concerning the spike onset speed. Fig. 2.6 illustrates the difference between models and neurons. McCormick et al. counters and attributes both phenomenons to the spike initiation site being located far inside the axon, and thus resulting in a slow spike onset as well as a high threshold variability in the measured back-propagating spike.

Because the project presented here is based solely on a phenomenological search based on the simple voltage trace, we can hardly use the findings presented here to bring the decision any forward. However, we can hope to have presented a tool that may contribute to the further discussion by allowing the precise determination of the SIPs for further analysis.

2.3.3 Late Spike Phenomenon

The late spike phenomenon is an interesting feature of the Hodgkin-Huxley type models that - to our knowledge - has not yet been described in the literature. It supports the view of a SIP as the “point of no return“: Once the SIP is crossed the model's trajectory will unavoidably run into a spike. This is exactly the behavior one would expect from a dynamical system when a separatrix is crossed: it will run into another attractor. We can thus see

this as another support for both the separatrix concept as well as the SIP concept presented in chapter 3.

Although this effect may seem bewildering it seems to be of no relevance for our analysis. Keeping in mind that models were noise-free and looking at the relevant time window (less than 1 μs of stimulus length decides about spike and no spike) it is a merely theoretical issue for dynamical systems theory.

Chapter 3

Neurons Have a 2-Dimensional Firing Threshold

3.1 Materials and Methods

3.1.1 Objective

In order to analyze cells for

- the existence of a threshold separatrix,

we will stimulate them with current ramps of different slopes, thus resulting in different slopes in intracellular U. In order to verify the results we will also test for

- the influence of an offset on the separatrix
- its temporal stability
- dependency on the A-type potassium current
- the separatrices of Hodgkin-Huxley type models

3.1.2 Cells

3.1.2.1 Animals

In vitro experiments were carried out on acute brain slices of the intact hippocampus region (containing CA1, CA3, DG, Subiculum) of adult ($>$ 7 weeks) wistar rats of both genders. The animals were bred at the animal husbandry of the Paul Ehrlich Center of Experimental Medicine at the Charité, Berlin, Germany. They were kept at an 12 hour light/dark cycle and had *ad libitum* access to food and water.

3.1.2.2 Slice Preparation

Rats were anesthetized in a big closable glass container (diameter about 25 cm, height 30 cm) using an ether atmosphere. The bottom of this container was covered with some layers of cellulose which were soaked with about 10 ml of ether. Rats were placed inside the container, and the lid was closed. When the overall body movements had seized and there was no more reaction to tilting the glass container, but the rat still showed clear respiratory movements, it was quickly decapitated using a rodent guillotine (in-house development of the Paul Ehrlich Center). The shading of the blood was used to verify sufficient oxygenation.

The next actions up to the cooling of the hemispheres in the vibratome chamber were carried out as fast as possible in order to minimize cellular damage due to hypoxia. First, the cranial skin was cut rostro-caudal along the medial line with a scalpel, starting between the eyes. Skin and fur were removed to uncover the cranium. Then the caudal part of the scull was cut at the caudal fontanel with a strong scalpel to remove the base of the scull. The lateral chewing muscles were cut at their cranial insertion points. With a strong pair of scissors, the cranium was opened on both sides, cutting just below the scull ridge. Care was taken not no damage the brain. Now the upper scull plate could be removed. The remains of the dura were carefully removed, the brain was then cut transversely just behind the bulbi olfactorii. Using a little spatula, the brain was removed from the scull and placed on a plane glass surface in its in vivo orientation.

Using a razor blade, the two hemispheres were separated by a sagittal cut. They were then tilted such that the formerly lateral side now pointed upward. Now the cranial cortex was removed (about 3 mm thick) on both hemispheres, and they were fixated with this freshly cut surface on the teflon block of a vibratome chamber using cyanoacrylate glue (UHU GmbH & Co. KG, Bühl, Germany). Now the ventral part of the brain pointed upward, and the cutting direction of the vibratome was latero-medial. The chamber was then filled with cool (4°C) and carbogenated (bubbled with carbogen gas, i.e. 5% CO_2 and 95% O_2, Messer Griesheim, Frankfurt, Germany [now Messer Group GmbH, Sulzbach, Germany]) artificial cerebrospinal fluid (ACSF) such that both hemispheres were fully submerged. From decapitation to here the procedure took about 3 minutes. The ACSF contained 124 mM NaCl, 1.25 mM NaH_2PO_4, 1.8 mM $MgSO_4$, 1.6 mM $CaCl_2 \cdot 2H_2O$, 3 mM KCl, 26 mM $NaHCO_3$, and 10 mM Glucose.

The brain was cut into slices of 400 μm using a vibratome (Campden Instruments Ltd., Loughborough, UK). The correct depth of the cutting plane was determined by visual inspection; only slices were used where both the

CA1/CA2 as well as the CA3 region of the hippocampus were clearly visible. Slices were trimmed, but the hippocampus' connections to the neighboring areas were left intact. Using a spatula and a soft brush (Rotmarder, size 3, Pelikan GmbH & Co. KG, Hannover, Germany [now Pelikan Holding AG, Schindellegi, Switzerland]) they were transferred onto little pieces of Kodak lens cleaning paper. These were then moved to an interface storage chamber for storage at room temperature. The storage chamber consisted of a block of acrylic glass with two milled-in interconnected caverns that were filled with ACSF. Slices were placed into one of the caverns on the fluid surface of the ACSF, supported by a tight grid of nylon stocking fabric. The atmosphere above the slices was moistened by carbogen gas that had bubbled through ACSF in the second cavern. Slices were left in the chamber for at least 1 hour before starting the experiments.

Some experiments and preparations were done in cooperation with G. Kreck.

3.1.2.3 Recording Electrodes

Recordings were made with intracellular sharp electrodes. These electrodes were freshly made before use (no electrode was older than 1 hour) from GB120F-10 filament borosilicate glass capillaries (Science Products GmbH, Hofheim, Germany), using a Flaming-Brown horizontal electrode puller (model P-87, Sutter Instruments, Novato, USA). The electrodes used showed a resistance of 50-100 MΩ. For recording, they were filled with fresh 2 M potassium acetate and checked for the absence of rectification. In later experiments, the electrode tip was carefully cleaned from bubbles using a heating wire under microscopic control.

3.1.2.4 The Experimental Setup

Experiments were carried out in an interface recording chamber (in-house development by U. Heinemann, based on a design of H.L. Haas [23], built in the Paul Ehrlich Center, Berlin, Germany) at 35°C slice temperature. This system was built from acrylic glass and consisted of a bath of aqua bidestillata with a thick acrylic glass cover. The water was heated by an electric foil heating to 37°C (heating unit and control unit developed and built in the Paul Ehrlich Center, Berlin, Germany) and bubbled by carbogen. Two experimenting chambers were milled into the cover, with little openings in their side through which the moistened and warmed carbogen (that had bubbled through the water) could sweep over the slices to provide a warm, O_2-rich and moist atmosphere. Each experimenting chamber had two nozzles at

the upper end through which carbogenated ACSF was supplied, and a sink on the opposite side. The ACSF feeding pipes lead through the water below, thus warming up the ACSF. Each experimenting chamber was equipped with two AgCl pellets as grounding electrodes. The interface chamber was fixated by permanent magnets on the heavy steel top of a active pneumatic experimenting table (Science Products GmbH, Hofheim, Germany) which isolated the setup from vibrations. The slice was illuminated by a cold light source (Olympus, Tokyo, Japan) via fiber optics. A stereo microscope (Leica Microsystems GmbH, Wetzlar, Germany) provided optical control of slice quality and coarse electrode position.

Before starting the experiment, the floor of the slice chamber was covered with one layer of lens cleaning paper (62647-B, Kodak, Rochester, New York, USA). For drainage, the inner chamber walls were aligned with 2 mm wide stripes of nylon stocking fabric which also led into the chamber's sink. Little sheets of Kodak lens cleaning paper of an appropriate layout ensured that the reference electrode pellets were in good electrical contact to the ACSF. The chamber was constantly flown through by carbogenated and warmed ACSF, supplied by a peristaltic pump (Minipuls 3, Gilson Inc., Middleton, UK) via the two nozzles at a rate of about 1.6 ml/min. For experiments, slices were transferred into the experimenting chamber on their little sheets of lens cleaning paper using a pair of tweezers and placed near to the ACSF supplying nozzle. For pharmacological experiments, the ACSF hose was removed from the standard ACSF reservoir and placed inside a second ACSF reservoir with added drugs. It took about 3 minutes for the new solution to reach the chamber's nozzle. Once a week, all components of the setup that come into contact with ACSF (hoses, storage chamber, experimenting chamber) were cleaned using a 0.3 M solution of H_2O_2.

3.1.2.5 Cell Search and Stimulus Parametrization

The electrode was positioned over the CA1 region where all cells were recorded. It was then lowered until electrical contact with the tissue was established. The bridge balance was adjusted at the amplifier to correct for the electrode's resistance. The capacity compensation was adjusted to correct for the electrode's capacity. During cell search, the electrode was lowered in steps of about 2 nm, using a mechanical 3D positioning device (Leica Microsystems GmbH, Wetzlar, Germany). To clean the electrode tip as well as to make cell penetration easier, the so-called buzz[1] was used frequently. This cell

[1]"Buzz" means a short increase of the capacity compensation, yielding to an oscillation of the compensation circuit. The processes leading to both an easier cell penetration as well as cleaning the electrode tip is not known, but it is a successful standard procedure

search procedure was done without microscopic control, i.e. "blind". Bridge balance and capacity compensation were permanently checked and adjusted if necessary.

While in the extracellular space, a repetitive hyperpolarizing pulse (amplitude 0.1 nA, duration 100 ms) was used with bridge balance slightly out of balance. Proximity of a cell was suspected when the apparent electrode resistance showed a sudden increase or when extracellular AP appeared. After penetration of a cell it was hyperpolarized in order to help the cell to recover from penetration. Under permanent control of the cellular health state the hyperpolarizing current was slowly reduced to 0. Cells were then given about 10-15 minutes time for accommodation and regeneration before starting any stimulation.

After this pause, they were roughly checked for firing threshold, resistance, time constant and spike amplitude. If these parameters seemed healthy (see 3.1.4.1 for healthy parameters), the cells were used for experiments.

First, the amplitudes of the depolarizing and hyperpolarizing offset currents were identified. The depolarizing offset amplitude was chosen to be slightly sub-threshold. The hyperpolarizing offset was chosen to be roughly 5-10 mV below the resting potential.

Now the slopes of the stimulus currents were defined from the resting potential. As the precise form of the membrane potential during a ramp could not be controlled, the membrane potential before the stimulus and the potential at spike initiation were used as as fixed points and a linear estimate was made. Stimulus slopes were now chosen such that the resulting estimated linear membrane potential slopes were roughly 0.1, 0.2, 0.4, 1.0, 2.0 mV/ms. This procedure was repeated for both offsets potentials in order to investigate the influence of the offset on the threshold.

3.1.2.6 Stimulation

Stimulus generation and data recording was controlled by an individually developed LabView program. It provided a graphical user interface for fast, easy and flexible access to all necessary parameters and controls. It also provided automatic mechanisms to assure that all relevant recording and stimulation parameters were saved in the data file header.

The computer-generated stimulus signals were digitized at 35 kHz in order to ensure high temporal precision even with fast signals. They were output via a data interface card (Type PCI MIO 16 E 4, National Instruments Corp., Austin, Texas, USA) and then amplified to comply with the needs of the

for sharp electrode recordings.

stimulus channel of the amplifier (Model IR-183, Neuro Data Instruments Corp., New York, USA), fed into it and applied to the cell through the recording electrode. Additionally, this stimulus output of the Neuro Data amplifier was recorded by the computer again (via the same card) and saved along with the cellular signal (one individual file per stimulus). Thus, the real stimulus is accessible at any part of the intracellular signal. Both the stimulus and the cellular signal were also displayed on an oscilloscope for online control.

The recorded intracellular membrane potential was fed into the Neuro Data amplifier via its high-resistance (about $10^{13}\,\Omega$) head stage pre-amplifier, low-pass filtered at 3 kHz, digitized at 35 kHz via the PCI card and stored on the computer's hard disk (Pentium III 700 MHz Processor, Windows NT). This high sampling rate was chosen in order to be able to precisely locate the start of the spike. As the spike start contains relatively low frequencies as compared to the filter's cut-off frequency, this does not interfere with the low-pass filtering.

3.1.2.7 *In Vitro* Experiments

After identification of all stimulus parameters for the individual cell the experiments could be started. At first the cell was stimulated by a 500 ms long positive square pulse, adjusted to an amplitude that initiated a sequence of spikes. In data analysis later on this served as an indicator for the cell type. Second, a sequence of 9 different 200 ms long square pulses with different sub-threshold positive and negative amplitudes was given, thus allowing to determine voltage/current relationship, the cell resistance and the time constant.

For each experimental run there were 5 different slopes to be tested at 3 different offsets (positive offset, resting potential and negative offset), i.e. 15 parameter combinations. Each parameter combination was given 10 times to enhance reliability, and the sequence of parameter sets was pseudo-randomly selected. There was a pause of at least 2 s between each parameter set to avoid any aftereffects of the previous stimulation (see fig. 3.1).

In case of stability analysis, this procedure was repeated after a pause in order to investigate temporal stability of the results. In case of pharmacological experiments, Drugs were added to the ACSF and perfusion was started at least 20 min before the actual measurement since diffusion into the slice is rather slow (see [35]). After that the procedure was repeated with the same stimulus parameters. After a pharmacological experiment, the slice was discarded and the chamber thoroughly washed with standard ACSF before using a new slice.

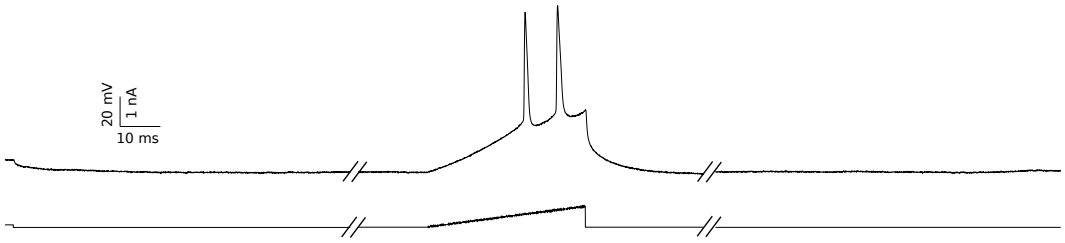

Figure 3.1: Scheme of a typical stimulation.
Lower trace shows the stimulus, starting (in this case) with an negative offset (left) of -100 pA. Upper trace shows the cell's answer. One stimulus run had the constant length of 1 second, which consisted of a 300 ms delay after the onset of an eventual offset, the ramp itself, and a trailing pause after which the offset was switched off (right side of figure). Between two stimuli there was a 2 second pause. Specifying an optional boundary allowed to start recording before and after the stimulus, i. e. before and after the offset. Typical stimulus slopes used were between 1.5 and 250 nA/s. Stimulus amplitude was 744 pA in this case.

For pharmacological experiments, the idea was to test the impact of the A-type potassium current on the firing threshold. In order to test this hypothesis, these channels were blocked using 50 μM 4-Aminopyridine (4-AP). Application of 4-AP with 50 µM affects (among others) K currents mediated by Kv1 and Kv3 channel members and can induce seizure like events. To prevent generation of epileptiform discharges synaptic transmission was blocked using a cocktail of glutamate and GABA receptor antagonists (30 μM CNQX (6-cyano-7-nitroquinoxaline-2,3-dione, a competitive AMPA/Kainate receptor antagonist), 60 μM APV ((2R)-amino-5-phosphonovaleric acid, a selective NMDA receptor antagonist), 5 μM Bicucullin (a competitive $GABA_A$ antagonist) and 1 μM CGP-55845A ([(2S)-3-[[(1S)-1-(3,4-dichlorophenyl)ethyl]amino]-2-hydroxypropyl](phenylmethyl) phosphinic acid, a $GABA_B$ antagonist)).

3.1.3 Models

3.1.3.1 Modified Leaky Integrate-And-Fire Model

The leaky integrate-and-fire (LIF) model was introduced by Lapicque in 1907 [29]. Contrary to the models of the Hodgkin-Huxley type, the LIF model is a simple one. It incorporates a constant capacity, a constant resistance and resembles a low-pass filter:

$$C\dot{U} + \frac{1}{R}(U - U_0) = I$$

This term computes the passive fluctuations of the membrane potential. In order to use it as a neuron model a threshold criterion is introduced:

$$U = U_0 \text{ if } U \geq U_\theta$$

Typically, it is equipped with a fixed voltage threshold, and its "membrane potential" is simply reset to a given value U_0 when the threshold is reached, i.e. no spike is produced. This is a problem for the questions to be investigated here as they explicitly need to look at the voltage trace exactly at the transition from the sub-threshold behavior to the spike behavior. Especially the SIP finding algorithm needs the spike upstroke to determine the SIP. In order to cope for this, an artificial analytical spike is attached to the model's voltage trace exactly at $U(t) = U_\theta$ (see left plot in fig. 3.2). Of course explicit care is taken to assure that there is a smooth transition from the model trace to the spike trace as this will be the point to be analyzed later. To do so, we determine the slope ($\frac{dU}{dt}$) of the voltage trace at $U(t) = U_\theta$ and find the attachment point with exactly the same slope within the onset of the artificial spike.

The artificial spike is an analytical function that has been precisely fitted to the onset and upstroke of a real spike according to the procedure described in [18]. It mimics the spike onset and upstroke in great detail (see right plot in fig. 3.2). In order to adopt it to the spike features (U and $\dot{U}$ amplitudes) of the data at hand it was compressed in the time domain by factor 2. This modification was used solely to make results comparable to the cellular data.

Within this simple model we are able to predefine arbitrary separatrices. We will thus be able to test the analytical algorithms used further on to check whether they are able to reproduce these built-in separatrices.

Three different threshold criteria were used for the leaky integrate-and-fire models:

1. Type A (exponential): $U_\Theta = \begin{cases} 1000 & \dot{U} \leq 0 \\ \exp\left(3 - 0.2\dot{U}\right) & \text{otherwise} \end{cases}$

2. Type B (root): $U_\Theta = \begin{cases} 1000 & \dot{U} \leq 0 \\ \sqrt{20\left(\dot{U} + 1\right)} & \text{otherwise} \end{cases}$

3. Type C (quasi linear): $U_\Theta = \begin{cases} 1000 & \dot{U} \leq 0 \\ 5 + 0.5\dot{U} & \text{otherwise} \end{cases}$

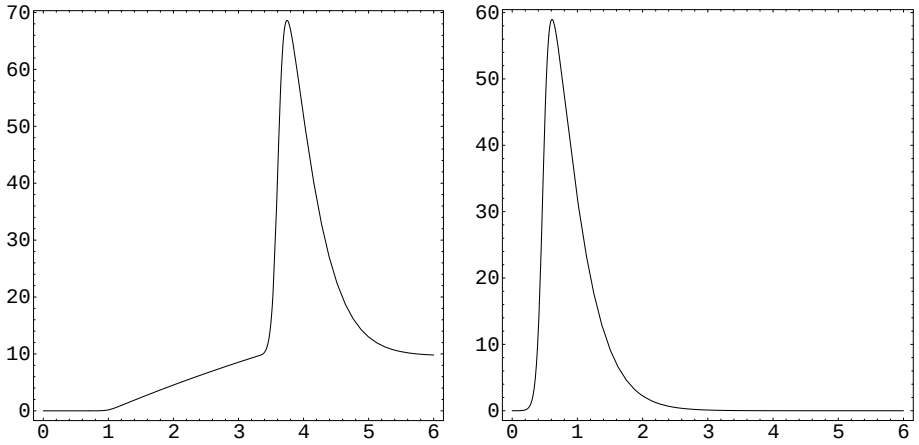

Figure 3.2: Behavior of the modified leaky integrate-and-fire model.
Left: when stimulated, the membrane potential of the model rises to the threshold value U_θ. While the original model would now simply reset the voltage to U_0, an analytically defined spike is attached to the voltage trace. It is taken care to assure that $\frac{dU}{dt}$ is exactly identical at the transition from model trace to spike trace. As we are only interested in the spike initiation we do not need to take care of the post-spike behavior of the model.
Right: The analytical spike that is attached to the model. The slope of the point of attachment on the spike is chosen to be exactly the same as on the model's voltage trace at $U(t) = U_\theta$.
Both figures show voltage [mV] against time [ms].

For easier comparison with cells and the other models the calculated voltage data of the leaky integrate-and-fire models were shifted to the mean membrane potential of all measured cells before analysis.

3.1.3.2 Hodgkin-Huxley-Model

The original Hodgkin-Huxley model ([24], used in the version from [28]) resulted from measurements that Hodgkin and Huxley had carried out on the giant axon of the squid. This and the fact that the measurements were done at low Ca^+ and at a temperature of 10°C indicate that there is a big difference in model behavior compared to a mammalian neuron at body temperature. Nevertheless, the Hodgkin-Huxley model is modeled because of its principle importance as a reference.

The central equation of the Hodgkin-Huxley model is the current balance equation $C_m \frac{dV}{dt} = I_{Na} + I_K + I_{leak} + I_{inj}$, that is it basically depends on the sum of all currents flowing in and out of the membrane, according to Kirchhoff's law. There is the sodium current I_{Na} and the potassium current I_K, both resembling the currents that flow through the corresponding ion channels, the leak current I_{leak}, indicating that the membrane is not hermetically sealed, and of course all currents injected into the cell via a stimulation electrode, I_{inj}.

For better comparison with cells and the other models the calculated voltage data of the Hodgkin-Huxley model was shifted to the mean membrane potential of all measured cells before analysis.

3.1.3.3 Wang-Buzsáki-Model

In 1996, Wang and Buzsáki [45] introduced a Hodgkin-Huxley type model of hippocampal interneurons. Their motivation was to investigate gamma oscillation in a hippocampal network model, so their current balance equation is $C_m \frac{dV}{dt} = I_{\mathrm{Na}} + I_{\mathrm{K}} + I_{\mathrm{syn}} + I_{\mathrm{leak}} + I_{\mathrm{inj}}$ with the synaptic input current I_{syn}. The modifications of the original Hodgkin-Huxley model were made in order to phenomenologically adjust the model behavior to the behavior of real interneurons in respect to an afterhyperpolarization and high firing rates. There is no need, however, to consider any synaptic input for this work, so the model falls back to the current balance equation known from the standard Hodgkin-Huxley model. The parametrization is, of course, different.

3.1.3.4 Awiszus-Model

In 1992, Awiszus [1] presented a modified Hodgkin-Huxley model. His intention was to adopt it to the behavior of a mammalian neuron at body

temperature. Basis for this modification was voltage-clamp data from small rat neurons in the supra-optic nucleus area [15, 14]. In this modification, an A-type potassium channel is added to the standard Hodgkin-Huxley model, so that the basic equation is $C_m \frac{dV}{dt} = I_{\mathrm{Na}} + I_{\mathrm{K}} + I_{\mathrm{A}} + I_{\mathrm{leak}} + I_{\mathrm{inj}}$. This family of models will allow to test the impact of the A-type potassium current.

3.1.3.5 Reduced Awiszus-Model

In his paper [1] Awiszus reduces the model from 6 to 5 dimensions by utilizing the close relationship of the variables a and h. In this 5-dimensional model, the corresponding equations are combined into one, thus reducing the dimensionality. All other equations are identical with the full model.

3.1.3.6 Modified Awiszus-Models

With the full Awiszus model modeling the A-type potassium channel, we have the ability to investigate the influence of this type of channel on the separatrix. We have thus modified the model by blocking the A-type potassium current. This is done by setting the maximum conductance for the A-type potassium channel to $\overline{G}_{\mathrm{A}} = 0\,\mathrm{mS/cm^2}$. As this modification resulted in a permanently spiking behavior at resting potential, we adjusted the leak current parameters to $\overline{G}_{\mathrm{leak}} = 0.1768\,\mathrm{mS/cm^2}$ and $E_{\mathrm{leak}} = -76.95\,\mathrm{mV}$ such that the model did not spike at rest. This model will be referred to as "NoA".

In order to provide a usable comparison for this modification we modified the full model to the same values for $\overline{G}_{\mathrm{leak}}$ and E_{leak}.

3.1.3.7 *In Silico* Experiments

The models were stimulated in the same way as the biological cells. Calculations were carried out on x86 computer architecture running Linux operating systems (RedHat Version 7.1 and 7.3, Suse Version 9.0, 9.1, 9.2, Ubuntu Version 8.9 and 9.1), using the Mathematica software package (Wolfram Research, Inc.) in versions 4 and 5. Models were numerically solved using the built-in numerical solver for differential equations with a maximal step size of 0.1 s.

Preliminary tests were conducted to check the influence of external noise on the separatrix. For these we recorded intracellular noise with the experimental setup and shifted its mean to 0. This noise was then used to noise the models by simply adding it onto the smooth model results. Further comparison between pure and noisy models revealed identical SIPs (and thus identical separatrices), so all further analysis was done with pure (i.e. noise-free) models.

3.1.4 Data Analysis

3.1.4.1 Cell Quality Criteria

Cells were only used for further analysis if they met the following quality criteria:

- spike amplitude more than 60 mV
- action potential overshooting
- membrane resistance more than 25 MΩ
- membrane time constant more than 2.5 ms

3.1.4.2 Data Postprocessing

The postprocessing procedure consisted of several self-developed Perl and Mathematica tools for automatized data preparation, arrangement and feature extraction. The aim of this process was to prepare and arrange the crucial data for easy, standardized and widely automatized access by the analysis programs. The following steps were applied:

1. unzip data file
2. read parameter header
3. find maximum of first spike during stimulus ramp
4. write relevant information into log file
5. re-zip data file

Using a self-developed Mathematica tool set, this extracted information was used to extract the relevant data (spikes as well as stimulus) from the raw data files and save them in a binary Mathematica format for easy and standardized access for all further analysis.

3.1.4.3 Data Analysis

All data have been processed in the same way, independent of their origin (cells or models). First of all, only the first spike on each ramp was used for further analysis in order to eliminate any spike aftereffects at the SIP. This spike was extracted from the original data file together with the corresponding stimulus trace. From this original voltage data the voltage derivative was calculated using the mean of three subsequent data points:

$\dot{U}_i = \frac{f}{1000}\left(\frac{U_{i+1}-U_{i-1}}{2}\right)$ with $\dot{U}_i$, the derivative of the i^{th} data value, U_i, the voltage value of the i^{th} data value, f, the sampling frequency, and i, the index. With the voltage given in mV this calculation yields the derivative in units of mV/ms. It is a simple algorithm for calculating the derivative for evenly spaced data, and it only makes a minor error within the 3-value data window. We also have tested more complex derivative filters like e.g. the Savitzky-Golay filter class, but there was no significant difference within the results.

Having U and $\dot{U}$, we can now use the algorithm described in 2 to precisely determine the SIPs of the spikes. All 10 SIPs generated with the same parameter combination were grouped together, and the center of gravity (2-dimensional mean) of each of these clouds was calculated together with the 2-dimensional standard deviation and standard error of mean (SEM). Models of course were calculated only once per parameter combination as they are completely deterministic. We fitted a function of the form $a_0 + a_1 x + a_2 \log(x)$ with $a_n \in \mathbb{R}$ to each state variable separately by minimizing the 2-dimensional distance of the function to the means. These fitted 2-dimensional function now is the separatrix of the cell.

3.2 Results

3.2.1 Cells

3.2.1.1 Separatrices

We have been able to record from 22 cells that met the quality criteria (see 3.1.4.1). Among these cells were 10 regular spiking, 5 oscillatory, and 6 fast spiking. One cell could not be clearly allocated to a special cell type by the recorded data.

The cells showed very different types of separatrices. They can be grouped into 4 groups:

- **vertical (n=6):** The vertical separatrix is the type of threshold one would expect from a cell with a pure voltage threshold. It varies in the $\dot{U}$ domain, but all spikes are elicited at the same voltage U.

- **horizontal (n=4):** This is the opposite of the vertical separatrix. All spikes start at the same $\dot{U}$ value, so effectively we have a $\dot{U}$ threshold. As a consequence, the SIPs span up to 20 mV, thus again strongly questioning the 1-dimensional threshold concept.

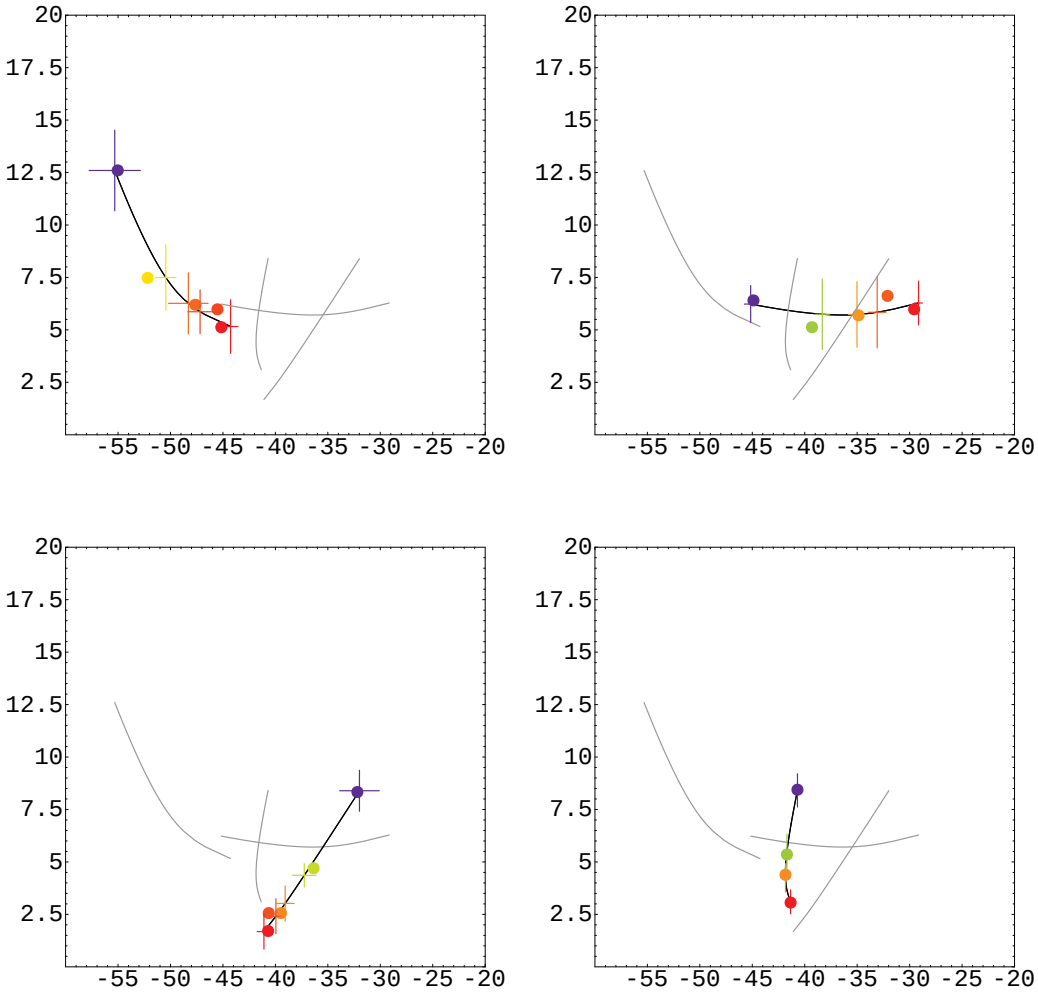

Figure 3.3: The 4 types of separatrices.
The cellular separatrices can be grouped into 4 types: horizontal (n=4), vertical (n=6), slash-type (n=7) and backslash-type (n=5). Note that the non-vertical separatrices span ranges of more than 15 mV, sometimes up to 30 mV (see next figure). The colored dots represent the means of all stimulus repetitions with the same parameters, the curves were fitted to these points. The SEM crosshairs have the corresponding color, they were projected onto the separatrix for better visibility. The color continuum codes for the slope of the stimulus ramp: from red (shallow ramps) via orange and green to blue (steep ramps). Note that same colors on different cells do not necessarily mean same slopes as ramps were individually adjusted and cell parameters were different for each cell.
Top left: backslash type separatrix, top right: horizontal type separatrix (pure $\dot{U}$ threshold), bottom left: slash type separatrix, bottom right: vertical type separatrix (pure U threshold).

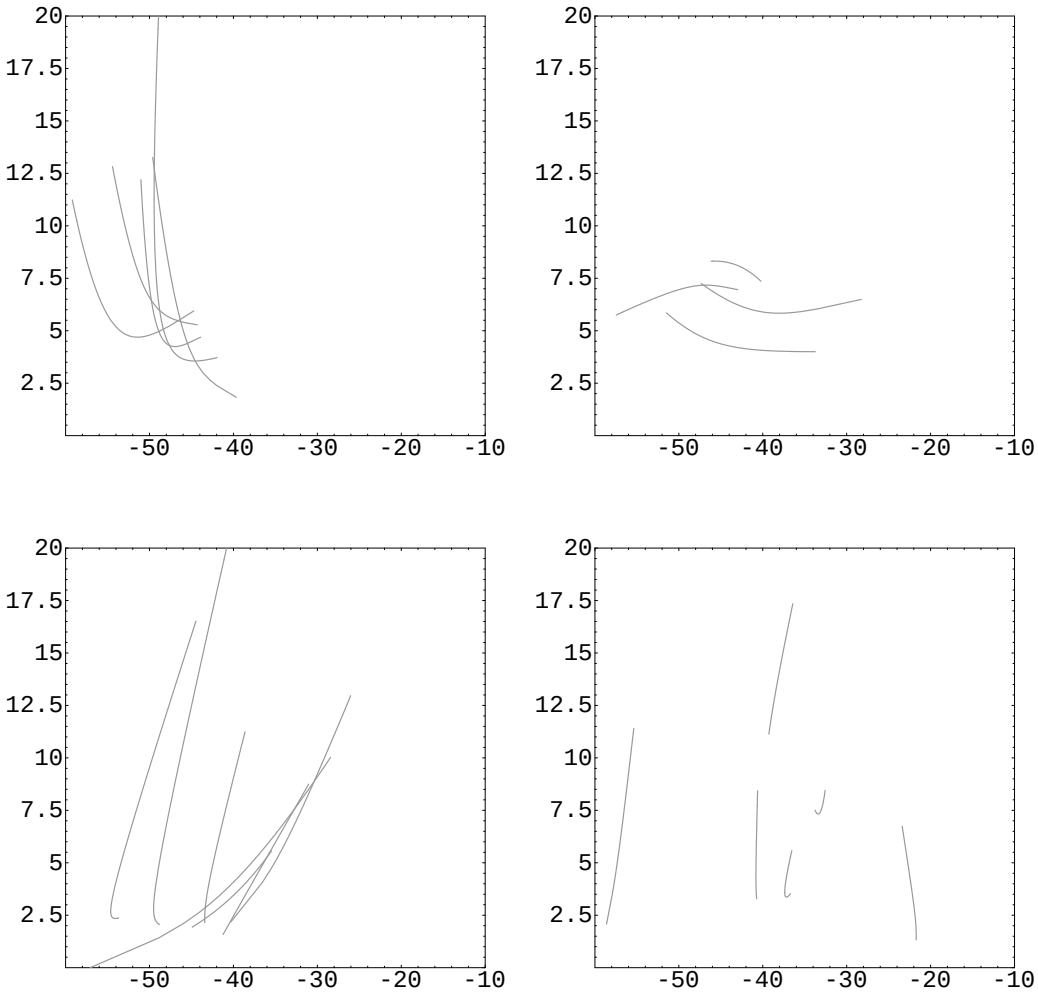

Figure 3.4: All measured separatrices.
This plot shows the separatrices of natural cells, grouped by their type: backslash-type (n=5, top left), horizontal (n=4, top right), slash-type (n=7, bottom left), vertical (n=6, bottom right). Note that sometimes the classification of a separatrix is difficult.
Top left: backslash type, top right: horizontal type (pure $\dot{U}$ threshold), bottom left: slash type, bottom right: vertical type (pure U threshold).

- **backslash (n=5):** Backslash-type separatrices show a behavior that has qualitatively been reported from cells before: shallow ramps have a higher U threshold value than steep ramps.
- **slash (n=7):** In slash-type neurons shallow ramps elicit spikes at lower voltages than steep ramps: this is somewhat contrary to the backslash type.

Note that this classification is merely conceptual. Neurons seem to show a continuum of separatrices, i.e. they can be any angle from horizontal via backslash-type and vertical to slash-type. Despite our efforts to find some correlation between separatrix type and some other cell parameters we did not succeed. We could neither establish a link between the separatrix form and the cell type.

3.2.1.2 Offset

The neuron's separatrices show no significant dependence on offset (see fig. 3.5). Thus, for the analysis of the cellular data we ignored the offset parameter and grouped data for each cell using the slope of the stimulus ramp. Control evaluations with the three offset data sets kept distinct showed no significant difference.

3.2.1.3 Stability and Sensitivity

Separatrices showed stability over time. In 5 cells we were able to repeat a complete stimulation set at least once. Comparison of the separatrices of healthy and stable[2] cells showed no difference (see fig 3.6, A and B). As long as the cell's relevant parameters are the same for each run, the separatrices are congruent or at least in very close proximity.

However, there are stability experiments where the separatrix is clearly shifted from run to run (see fig. 3.6, C). Searching for the cause of this shifts we find that some of the monitored cell parameters have slightly changed: membrane time constant, membrane resistance, spike amplitude. Being unable to prove any causal connection between these two effects due to insufficient data this phenomenon shall simply be stated here (see section 3.2.1.4 for similar findings).

[2]A cell is considered stable if their relevant state parameters (spike amplitude, resting potential, membrane time constant etc.) were identical to the initial values in all successive trials.

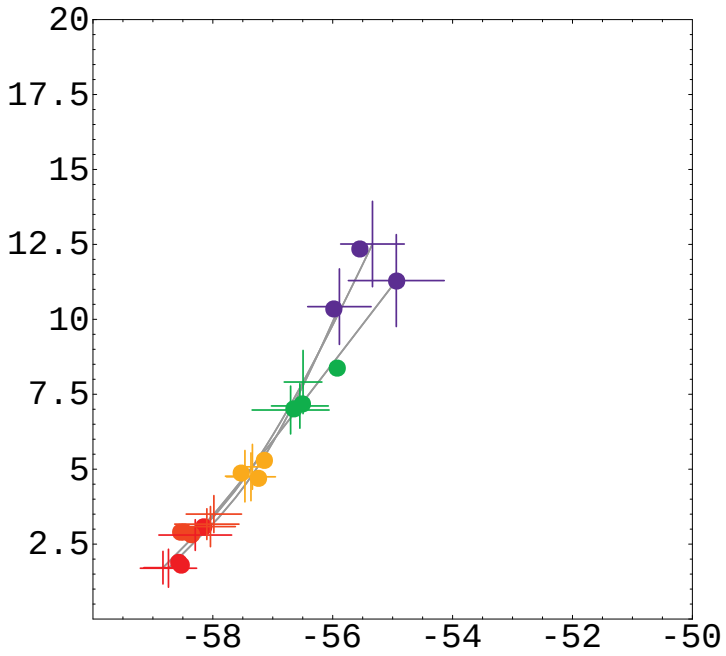

Figure 3.5: Neural separatrices are insensitive to offset.
These three separatrices from the same cell were generated from the resting potential, from a -10 mV hyperpolarized state, and from a +5 mV depolarized membrane potential. They are congruent.
Crosses show the SEM of the means, projected onto the separatrices, and dots show the means of the SIPs elicited by the same stimulus slope. Colors of crosses and dots code for the slope of the stimulus from shallow (red) to steep (blue). Axes are $\dot{U}$ [mV/ms] against U [mV].

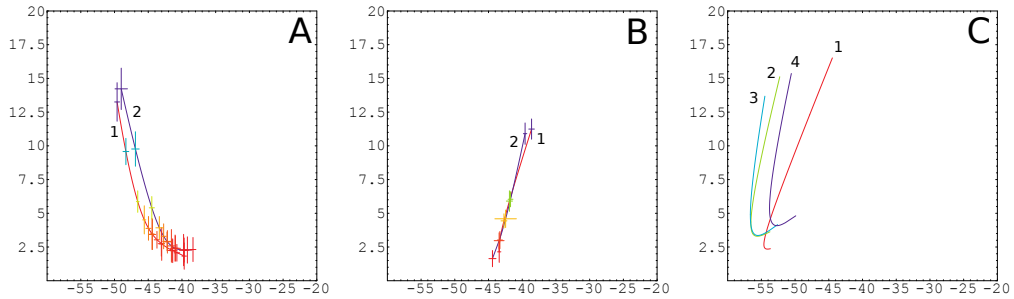

Figure 3.6: Separatrix temporal stability and sensitivity.
Left plot (A): This neuron initially displays the red separatrix (1). After 30 min the same stimulation set is repeated, resulting in the blue separatrix (2). Both separatrices show an identical form and are nearly congruent. However, the small change may be due to an increase in membrane resistance (+2 MΩ) as well as an decrease in spike amplitude (-3 mV). Middle plot (B): This neuron was tested with two runs 10 min apart: both separatrices (red (1): first, blue (2): second) are perfectly congruent. All cell parameters recorded here are identical between the two runs. Right plot (C): this neuron showed the red separatrix (1) in the first run and was tested again after 20 (green, 2), 40 (turquoise, 3) and 60 (blue, 4) min, showing clear differences. Looking at the other relevant cell parameters, we see a continuous reduction in membrane resistance (-2 / -1 / -1 MΩ) as well as slight changes in spike amplitude (-1 / -1 / ±0 mV).
Crosshairs show the SEM of the means, projected onto the separatrices, the means of the SIPs are omitted in order to enhance visibility. Colors of crosshairs code for the slope of the stimulus from shallow (red) to steep (blue). Colors of separatrices in all 3 plots are solely for better distinguishability and do not code for any parameter. Axes show $\dot{U}$ [mV/ms] against U [mV].

3.2.1.4 Pharmacology

With 5 cells we were able to conduct pharmacological experiments. As a result we cannot verify any effect of a pharmacological block of the A-type potassium channels on the separatrix. However, another effect was visible (and possibly shadowed any 4-AP effect) within these experiments: the separatrices react very sensitive already to the application of the synaptic block cocktail alone. (see fig. 3.7).

As the hippocampal collaterals are intact it is necessary to provide a synaptic block previous to the A-type channel block in order to avoid seizure-like events due to reduced potassium conductance. This block (see 3.1.2.7) already shifted the separatrix significantly.

From the 5 cells treated pharmacologically 3 had a rather vertical initial separatrix (see fig. 3.7 A and B for examples), and the remaining two had a mainly horizontal one (one displayed in fig. 3.7 C). All vertical separatrices showed a right-shift of about 3-5 mV towards higher voltage, both after adding the block cocktail alone as well as after adding block+4-AP. The horizontal separatrices exhibit a less obvious right-shift, and they additionally showed a downshift of up to 3 mV/ms. With all cells tested the blue SIPs, induced by steep ramps, shift more clearly than the red ones (shallow ramps). Washing out the pharmacological substances was not able to restore the separatrix to its initial position.

3.2.2 Models

3.2.2.1 Correctness of Separatrix Construction

With the modified leaky integrate-and-fire models having been constructed with pre-defined separatrices, we have the chance to test the separatrix construction algorithm. It turned out that it precisely reproduced the predefined separatrices. This confirms our approach to use the presented algorithm to reproduce the (phenomenological) separatrix.

3.2.2.2 Separatrices

The Hodgkin-Huxley type models showed backslash-type separatrices (see fig. 3.10 to 3.9). They were different between models in detailed form (curvature) or steepness, but none of them was found to show a horizontal or slash-type separatrix. The Wang-Buzsáki model was the only one showing a nearly vertical separatrix.

Some models (original Hodgkin-Huxley, Wang-Buzsáki) showed clear oscillations on ramp stimulation which one could imagine to distort precise

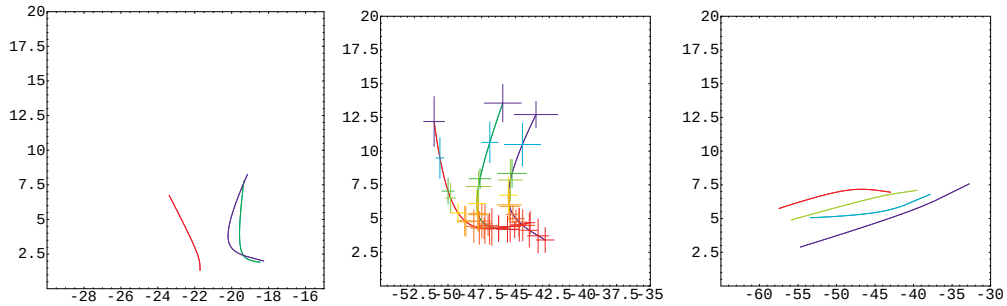

Figure 3.7: The separatrix is a sensible indicator of the cell's state.
Left plot: The separatrix seems to be a very sensible indicator of the cell's physiological state. This fast spiking neuron initially showed the red separatrix without any pharmacology. Second, the green separatrix was measured 30 min after application of the synaptic block cocktail without 4-AP. This already shifted the separatrix 3 mV to the left. Third, the additional application of 4-AP did not change it from its shifted state. Additionally, the following cell parameters changed between runs: membrane resistance +5 / +1 MΩ, spike amplitude -4 / ±0 mV. Middle plot: A regular spiking neuron. Red: The initial separatrix. Green: After 20 min under block+4-AP. Blue: After 50 min under block+4-AP. Additionally, the following cell parameters changed between runs: membrane time constant -1 / -2 ms, membrane resistance -4 / -12 MΩ, spike amplitude +4 / ±0 mV. C: Fast spiking neuron with its initial red separatrix, the green after 35 min under block+4-AP, the turquoise after 70 min under block+4-AP, the blue after 35 min wash. Additionally, the following cell parameters changed between runs: membrane time constant -2 / ±0 / -2 ms, membrane resistance +1 / +1 / +4 MΩ, spike amplitude ±0 / +1 / -11 mV.
Crosshairs show the SEM of the means, projected onto the separatrices, the means of the SIPs are omitted for better visibility. Crosshairs of left and right plots have been omitted for the same reason. Colors of crosshairs code for the slope of the stimulus from shallow (red) to steep (blue). Colors of separatrices in all 3 plots are solely for better distinguishability and do not code for any parameter. Axes show $\dot{U}$ [mV/ms] against U [mV].

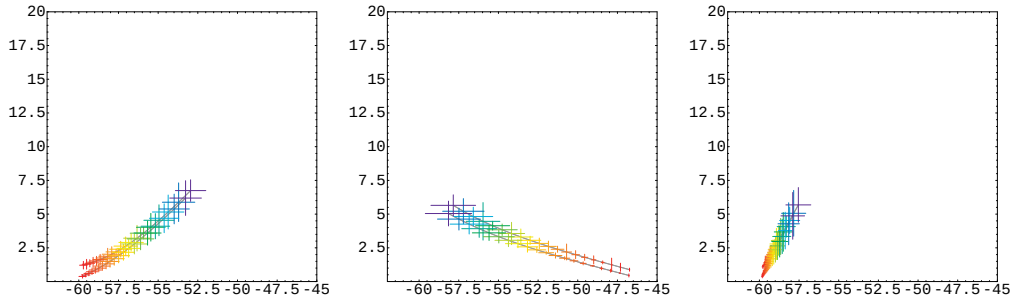

Figure 3.8: Algorithm can reproduce real separatrices.
Real vs. reconstructed separatrices of the 3 different predefined separatrix types in the LIF models (see 3.1.3.1). Left: type A, middle: type B, right: type C. The small deviations of the reconstructed separatrices are due to the limited temporal resolution because of the sampled model signal as well as to a systematic effect of the SIP finder (see 2). The leftmost separatrix is the real separatrix, while the found one is slightly more right. However, they are near enough to show that the algorithm presented here is able to phenomenologically reproduce a built-in separatrix.

detection of the SIPs and thus the separatrices. However, as the state space is spanned by U and $\dot{U}$, any distortion of the voltage trace before the SIP will simply shift the SIP along the separatrix without altering its form.

3.2.2.3 Real vs. Found Separatrices

Using the models, we are able to determine the real SIPs (and thus the real separatrices) via a second method (see chapter 2). Depending on the abruptness of the spike onset we see a significant divergence between real and found separatrices. Please refer to 2.1.1 for the results concerning real vs. found SIPs.

3.2.2.4 Offset

The separatrices of the modified Leaky Integrate-and-Fire models are - by definition - independent of the offset. Of course different offsets lead to different SIPs, especially because identical stimulus slopes lead to different voltage slopes at the SIPs. However, as the predefined threshold is independent of any other parameters but U and $\dot{U}$, these effects merely shift the SIPs along the separatrix (see the SEM ellipses elongated along the separatrix in fig. 3.10).

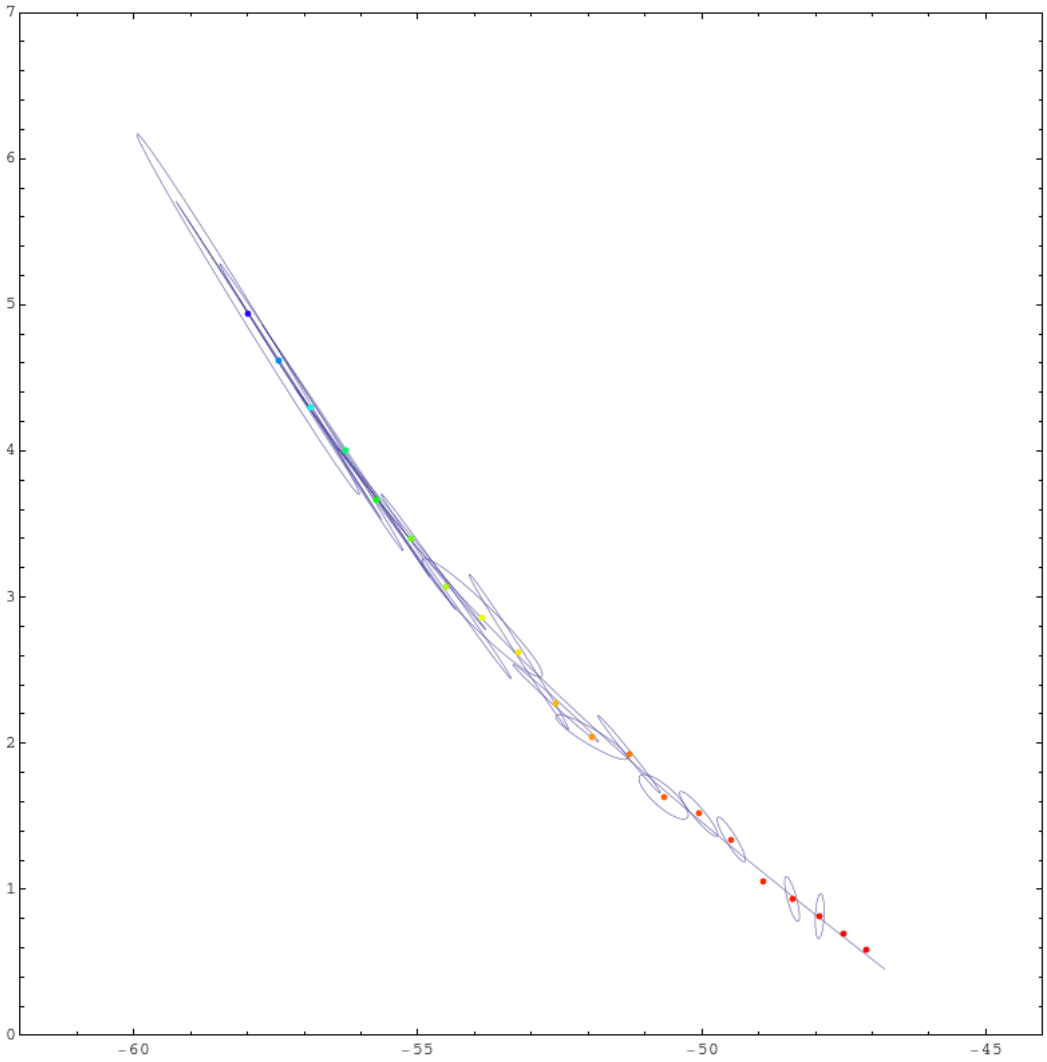

Figure 3.9: Offset dependence in LIF models.
The separatrices of the leaky integrate-and-fire models are *per definitionem* independent of the offset. This Figure shows the real separatrix of the type A model (see 3.1.3.1), with all offsets grouped together. Shifts occur at the steeper parts of the separatrix, but the orientation of the standard deviation ellipses show that they follow the separatrix itself, thus retaining its form. Dots denote the SIPs for the different stimulus ramp slopes, with the color shifting from red (shallow ramps) to blue (steep ramps), ellipsoids show the SEM. Axes are $\dot{U}$ [mV/ms] against U [mV].

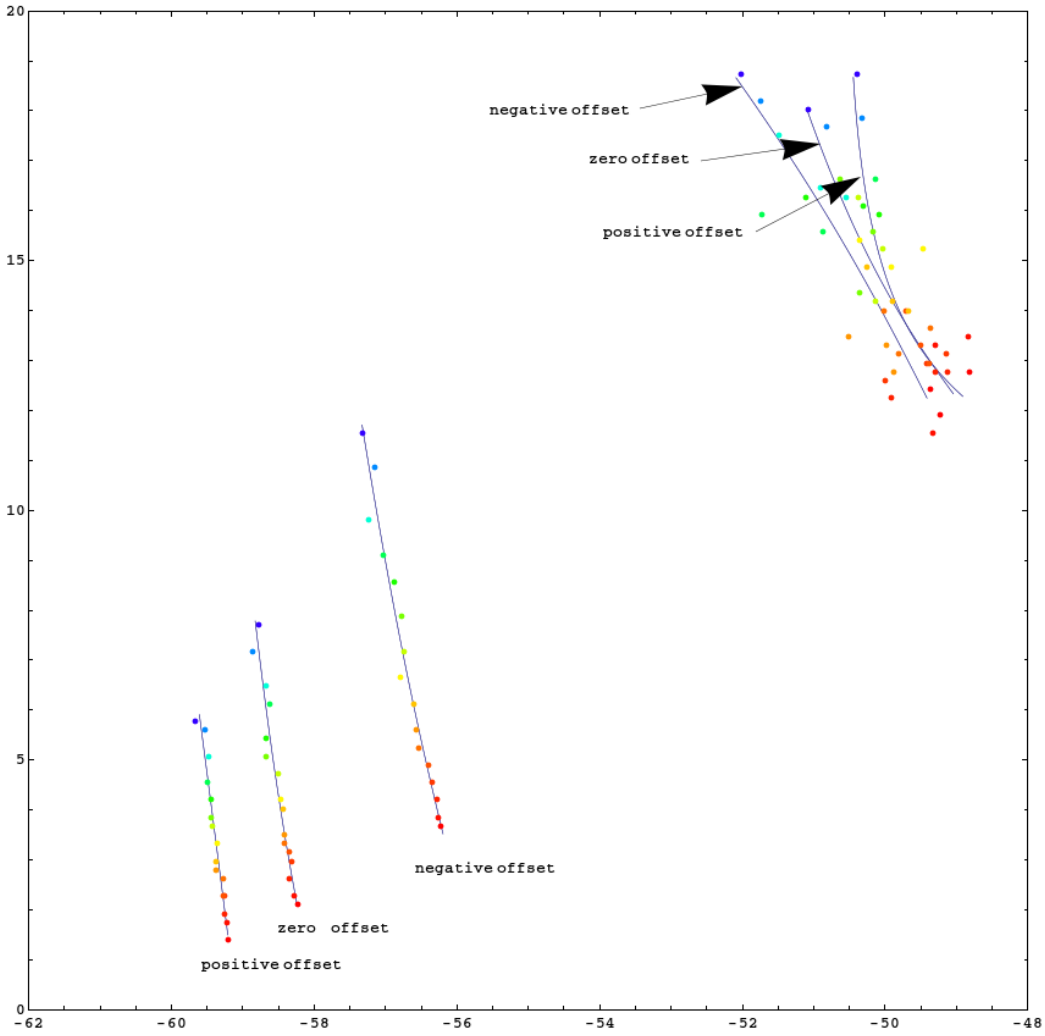

Figure 3.10: Offset dependence of the Wang-Buzsáki model separatrices.
The Wang-Buzsáki modification of the Hodgkin-Huxley model as an example for the offset dependence of the separatrix. The three distinct lines in the bottom left corner show the real separatrices, found via the ramp shortening paradigm (see 2.1.2). The upper right corner shows the three corresponding found separatrices, determined by the SIP detection algorithm presented in 2. The increased variability of the SIPs at the found separatrices is due to the much faster dynamic at this point.
Dots denote the SIPs for the different stimulus ramp slopes, with the color shifting from red (shallow ramps) to blue (steep ramps). Axes are $\dot{U}$ [mV/ms] against U [mV].

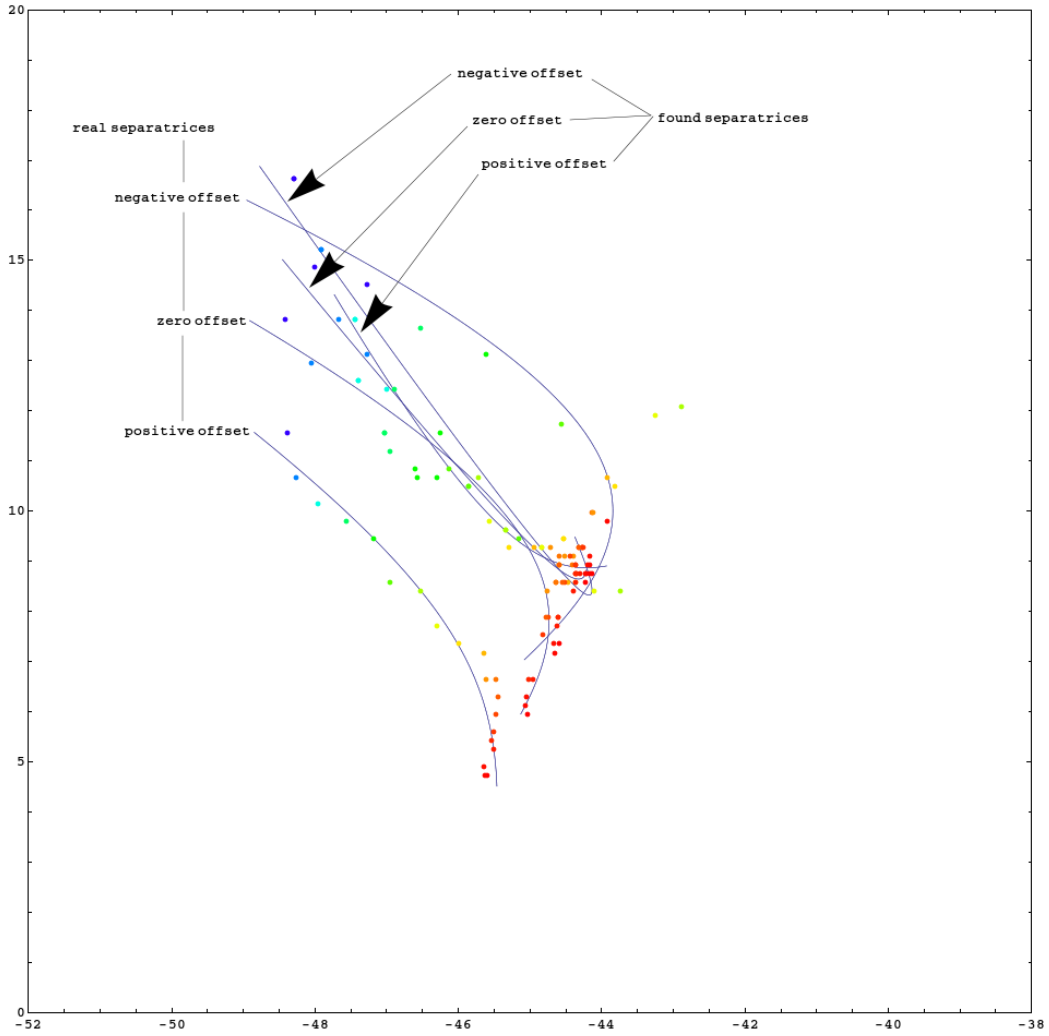

Figure 3.11: Offset dependence of modified Awiszus model separatrices.
The modified Awiszus model in the same layout. Note that the three detected separatrices are close to the real separatrices. Also note that the orientation and overall form of the found separatrices are identical to the real separatrices, although they are shifted in state space.
Dots denote the SIPs for the different stimulus ramp slopes, with the color shifting from red (shallow ramps) to blue (steep ramps). Axes are $\dot{U}$ [mV/ms] against U [mV].

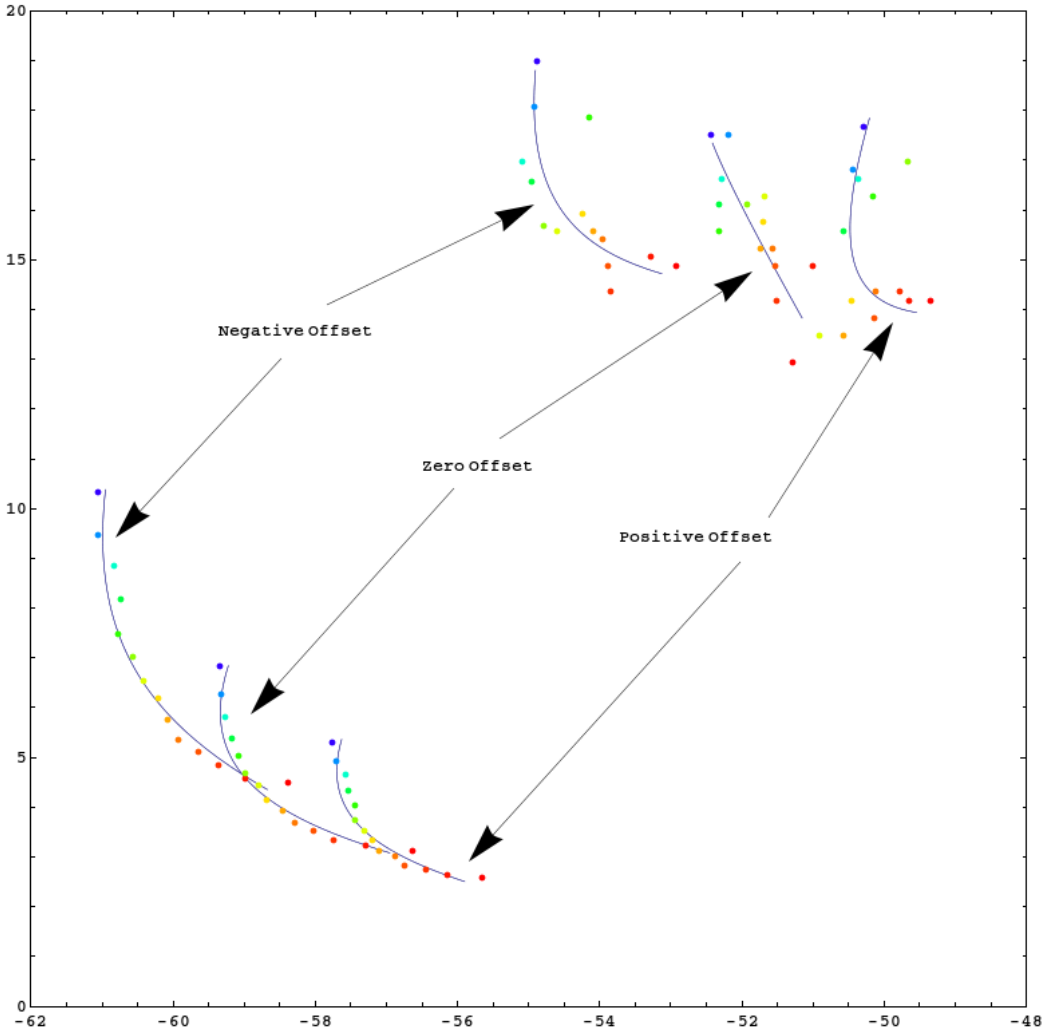

Figure 3.12: Offset dependence of Hodgkin-Huxley model separatrices.
The original Hodgkin-Huxley model shows a similar, but slightly different behavior. Instead of the three offset separatrices being shifted along the trajectories they are shifted perpendicular. However, we again find the found separatrices to be shifted along the trajectories, thereby reproducing the real ones.
Dots denote the SIPs for the different stimulus ramp slopes, with the color shifting from red (shallow ramps) to blue (steep ramps). Axes are $\dot{U}$ [mV/ms] against U [mV].

The Hodgkin-Huxley models are clearly sensitive to offsets, independent of their flavor. Within all of these models we see the three real separatrices for positive, zero and negative offsets clearly separated. For the original Hodgkin-Huxley model the different offsets shift the separatrices *perpendicular* to the course of the trajectories (see fig. 3.10 C), with the negative offsets inducing the upper and positive ones inducing the lower separatrix. This again also means that in this case the offset shifts the *course* of the trajectories. For all other Hodgkin-Huxley flavors tested here, the separatrices are shifted *along* the trajectories. Contrary to the original model this indicates that the offset does *not* change the course of the trajectories. In these models the rightmost separatrix is elicited from a hyperpolarized model, the middle one from a model at resting potential, the leftmost from a depolarized model. All models however show that the overall form of the real separatrix is retained in any case, independent of the offset.

The separatrices found by the SIP detector (see 2) typically lie far more right (i.e. shifted forward in time along the trajectories) than the real ones, meaning that they are detected significantly after their real occurrence. Only for the modified Awiszus model we find the detected separatrix within the range of the real separatrices. The temporal difference between real and found separatrices is directly linked to the abruptness of the spike emerging from the pre-spike dynamics: the smoother (i.e. less kinky) the spikes emerge (see fig. 2.5 for a comparison), the more distant the found separatrices are from the real ones, and vice versa.

It is worth noting again that the phenomenological separatrices found by the algorithms and procedures presented in this work are able to reproduce the key features of the separatrices in any case, be it angle, extension and curvature. As the amount of divergence of real to found separatrices is clearly linked to the sharpness of the trajectory's kink at spike onset, this again nourishes the view that our algorithm can be able to precisely identify the separatrices of real neurons as well.

3.2.2.5 Blocking the A-type Potassium Channel

With the A-type current being explicitly available in the Awiszus model, we can test the model's response to completely blocking the A-type current. To do so we have to compare the modified Awiszus model (NoA) with the modified Awiszus model with implemented A-type current as these two differ only in their A-type channel conductance.

While the found and real separatrices are rather close for the full model they are again clearly separated for the NoA model. As another support of our finding that the proximity of real and found separatrices is linked to the

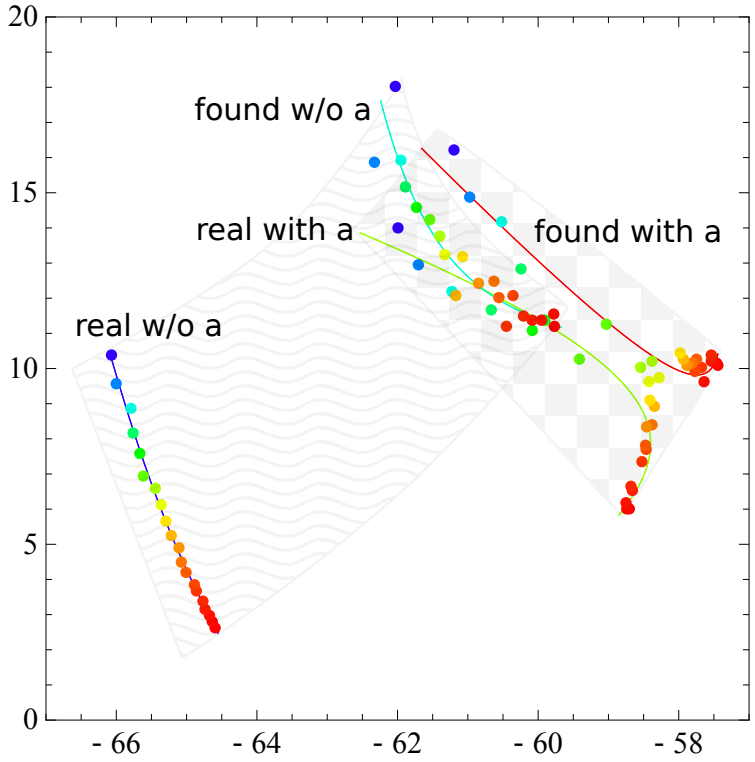

Figure 3.13: Modeled A-type channel block.
The red and green separatrices are the found and real ones of the control model with working A-type channel, the turquoise and blue separatrices belong to the model with blocked A-type channel. The comparison of the real separatrices of the two models (green vs. blue) shows a significant left-and-down shift (-5 mV, -4 mV/ms) together with a straightening. The found separatrices are in close proximity and show just a small left-and-up shift (-1.5 mV, +1.5 mV/ms). Note that the overall angle of tilt is preserved for all 4 separatrices.
The gray areas indicate the approximate corridor of the trajectories bundle. The waved area interconnects the two separatrices of the model without the A-type current, and the checkered one interconnects the two separatrices of the model with the A-type current. The checkered corridor is shifted a little to the lower right side, thus indicating that the model with the A-type current shows a slightly slower dynamic.
Dots show the means of the SIPs elicited by the same stimulus slope. Colors of dots code for the slope of the stimulus from shallow (red) to steep (blue). Colors of separatrices are solely for better distinguishability and do not code for any parameter. Axes are $\dot{U}$ [mV/ms] against U [mV].

abruptness of the spike onset, the full model turns in deed out to have a faster spike onset than the NoA version.

Looking at the found separatrices, we find a slight right-shift as well as a slight down-shift for the NoA Version as compared to the full model. This result is similar to the results found for the neurons (see section 3.2.1.4). However, the neurons showed this effect already when the synaptic block cocktail was added, there was no systematic 4-AP-related effect visible.

A more reliable result for the models is of course the real separatrix. Here we see a clear shift of about 5 mV to the right and about 3 mV/ms upward. The increased variability of the rSIPs (see green separatrix in fig. 3.13) indicates that the spike dynamic becomes irreversible later, closer to the fSIP separatrix. The real separatrix becomes curved, but maintains its overall orientation. Looking at the corridors of the trajectories bundle, it seems that the separatrix is not detected earlier, but the models spike dynamic becomes later irreversible.

However, due to obscure pharmacological results with neurons we are unable to link these findings to biology.

3.3 Discussion

The results presented in this work support the hypothesis (see 1.1) of $\dot{U}$ as a second state variable, resulting in a 2-dimensional firing threshold. These thresholds can be seen as separatrices in an U-$\dot{U}$ statespace projection which separate the passive pre-spike regime from the active spike dynamic. These separatrices are able to explain the (voltage) threshold variability found in typical intracellular spike recordings, thus making the new threshold concept much more adequate as compared to the 1-dimensional one.

We could also show that the algorithms presented here are able to precisely reproduce built-in separatrices from modified leaky integrate-and-fire models. Applied to neural intracellular recordings, we additionally could show that neurons have various types of separatrices: vertical, horizontal, slash-type, backslash-type. However, these types are not distinctly segregated, but they seem to form a kind of separatrix-continuum.

Furthermore separatrices seem to be a highly sensible indicator not only for the cellular health state, but also for small changes in spike-relevant cell parameters. In this context we could not verify any effect of an A-type potassium channel block.

Approaches to attribute certain cell types to certain separatrix types did not succeed. We have not been able to map the separatrix type to the cell type.

3.3.1 Model Separatrices

The separatrices of the leaky Integrate-and-Fire models precisely reproduce the built-in separatrices. This was to be expected as both the detecting algorithm as well as the predefined threshold function work solely in the phenomenological domain. It is, however, a proof for the ability of the algorithm to precisely detect the phenomenological SIPs.

The Hodgkin-Huxley separatrices show a more complex situation. Here we see a clear dependence on the starting membrane potential (depolarized, hyperpolarized, rest). This feature is present throughout all Hodgkin-Huxley models tested, but we find one difference: while the original Hodgkin-Huxley model has the three offset-related separatrices shifted along their longitudinal axis, all other flavors of the Hodgkin-Huxley model have their offset-related separatrices shifted along the spike trajectory (see fig. 3.10).

Additionally, the found separatrices are unable to reproduce any offset-induced shift along the spike trajectories that occurs in the respective models. In the contrary, they are all grouped more or less together. The exception is the original Hodgkin-Huxley model: Here we see the same shift in the found separatrices that is present in the real separatrices. However, this was to be expected as all separatrices are *per definitionem* located on the trajectory bundle. If a different offset shifts the trajectory bundle perpendicular to the trajectory direction, the separatrices - real as well as found ones - will be shifted as well.

It is an interesting finding that Hodgkin-Huxley models seem to exhibit mainly the backslash-type separatrices (although some are admittedly nearly vertical). Although the models tested here were designed with different intentions there is none among them that would show a different separatrix type. Even further parameter variation did not result in any other separatrix form. It would thus surely be an interesting approach to analyze systematically if and under which conditions Hodgkin-Huxley models are able to switch their separatrix into another type.

3.3.2 Separatrices in General

The idea of analyzing neural activity using phase plane projections is not new. It has been used in various mathematical papers (see e.g. [19] and the detailed works of Izhikevich, e.g. [25, 26]) in order to visualize neural behavior in the voltage as well as in the frequency domain using the concepts of limit cycles, attractors, bifurcations and thus even separatrices. However, this approach results from the theoretical *analysis* of the neuron as a dynamical system. Thus, even if the voltage U is used as one state variable, the other

one typically is a more abstract concept like an inactivation variable or the like.

The separatrix concept presented here is a much more phenomenological one. As already stated in the introduction (see chapter 1) the idea was to *construct* the separatrix by an experimental approach with an extension of the threshold concept in mind. This lead us to the combination of U and $\dot{U}$ as state variables, and the constructive experimental concept distinguishes the two approaches profoundly.

Although the separatrix algorithm reproduces the principal orientation of the real model separatrices, it fails to precisely locate the real model separatrices within the state space as well as their detailed curvature. As we have shown the distance between found and real separatrices is large for models with a slow spike onset and small or zero for models with a fast onset. Because the SIP detector works purely phenomenologically it *per se* cannot capture events that do not instantly show a significant effect on the membrane potential. Thus, we cannot precisely reproduce the real model separatrices with the algorithm presented here in most cases (because of the missing kink at spike onset in most models). We can, however, reliably reproduce the type (see 3.2.1.1) of the real separatrices as well as their slope.

While models make it easy to compare real and found separatrices, we have a different situation with the neurons. Here we have no chance[3] to reliably determine the "real" SIPs, not to talk about the corresponding separatrices. However, using the LIF models with predefined separatrices and attached physiological spikes, we were able to reproduce the built-in separatrices precisely. Thus it seems reasonable to extrapolate from models to cells - which means we can expect the found separatrices to reproduce at least the principal orientation of the cell's real separatrices, if not even their position.

The separatrix concept of spike initiation touches the current debate between Naundorf et al. ([36, 37]) and McCormick et al. ([33, 46]). Naundorf criticizes the Hodgkin-Huxley model for its slow spike onset dynamic as well as for not reproducing the high threshold variability of real neurons. McCormick argues that both features are due to the spike initiation site being quite far from the soma inside the axon. As a consequence, intracellular recordings would only capture back-propagated spikes. These would then show the two features - kink and threshold variability - because of changing electrophysiological properties on the transition from the narrow axonal spike initiation site to the much wider soma. In McCormick's view the Hodgkin-Huxley properties - slow spike onset and precise threshold - would nevertheless hold at the axonal spike initiation site.

[3] At least not with the techniques used in this study

However, we have shown here that there is also a significant amount of threshold variability (about 6 mV with the ramps and offsets used here) within the Hodgkin-Huxley model. We have also shown that based on intracellularly recorded voltage traces, cells exhibit a variety of separatrices whereas Hodgkin-Huxley models solely show the backslash-type. Although we cannot counter the distant spike initiation argument with the data at hand, these findings might hint to some missing feature within the Hodgkin-Huxley model. It would thus surely be fascinating to expand the separatrix concept to spatially distributed multi-compartment neuron models.

The work of Azouz et al. ([2, 3, 4]) has shown how threshold variability may be a relevant mechanism of neurons to allow precise synchronization of synfire chains for many purposes. They state that cells show a lower threshold for rapid (i.e. steep) depolarizations and a higher threshold for slow (shallow) ones. When cells encounter high-frequency membrane potential fluctuations they will thus be able to fire in high temporal precision as the rapid fluctuations will more likely produce a spike due to the low threshold. This view translated to the separatrix concept would mean a backslash-type separatrix with steep ramps eliciting spikes at lower voltages than shallow ramps.

Consequently, one has to expect other separatrices to exhibit other functional features. Slash-type cells would be the antipodal to this behavior, eliciting spikes more easily for shallow ramps than for steep ones. Horizontal separatrices would drive the idea of Azouz et al. to the extreme: These cells would fire mainly independent of the voltage, mainly depending on $\dot{U}$. And finally we have of course cells with a vertical separatrix that would exhibit a pure voltage threshold that has served as a suitable neural model trough decades.

Summing up all these considerations, we have to conclude that cells can exhibit a variety of functions within their interconnectivity network, and that it is surely imaginable that different functions are directly correlated to different separatrices.

3.3.3 Sensitivity

As was stated above we can show that separatrices are temporally very stable as long as the cell's parameters are constant. On the other hand we do occasionally see separatrices shifting from run to run. When searching for the cause of this shift we see slight changes in the monitored cell parameters. These changes are so small that normally they would seem to be unworthy looking at.

But during the pharmacological experiments we encountered another un-

expected result: separatrices shift already when the synaptic block cocktail is added. Searching for the causes we again find that the monitored cell parameters have changed a little bit.

Per se there are three possibilities for this effect: Either there is some slow shift within the technical recording sequence, or there are physiological changes within the cell due to fatigue or damage, or the cell may be actively shifting its separatrix.

The first point should be no cause, as we of course are trying to eliminate all technically induced biases. However, in further experiments extra care should be taken on this issue. The second and third possibility are hard to distinguish. In case of fatigue or damage one would surely expect one of the monitored cell parameters to reflect such changes. This is also likely, but not that clear, for some active shifting process. If the cell should really be able to shift its separatrix there may be parameters involved that are not monitored within the standard recording procedure.

In order to keep things as simple as possible we can only state that there are slight parameter changes visible whenever separatrices change - and on the other hand that they do not change when the separatrices stay congruent. This however would mean that the separatrix is a highly sensible indicator for the cell's physiological state.

3.3.4 Pharmacology

Recent work of Sonner and Stern [41] have investigated the properties of isolated A-type potassium channels. They have shown the 10-90% rise time of the A-type potassium current to be 6.1±0.4 ms which is - as compared to the spike speed - relatively slow.

If we now follow the argumentation that for fast spike dynamics the found separatrices are likely to be identical to the real separatrices (see fig. 3.11), this slow rise time can be taken as another support for this view. If the real separatrix was significantly earlier than the found ones (within the Hodgkin-Huxley models, we have found temporal differences of more than 1 ms), then an effect of the slower and smaller potassium current in the neurons treated with 4-AP would have to be expected at the SIPs. However, we are unable to attribute any of the visible effects clearly to 4-AP (see discussion of the results in 3.2.1.4) as we are unable to distinguish between effects of the block cocktail alone and 4-AP. It would therefore be adventurous to conclude any support or falsification for the separatrix concept from the pharmacological findings.

The modeled A-type channel block shows two effects (see fig. 3.13): first, the models trajectory bundle shifts up-left due to a modified dynamic, and

second, the real separatrix shifts further away from the found one (i.e. spikes become irreversible at an earlier point).

This behavior does not match any of the effects observed in the cells treated with 4-AP. In order to establish such a link between models and biology a much more solid data base would be necessary, with statistically verified effects. Unfortunately, this is not available from the data at hand, but remains an issue for further investigations. Additionally, an explanation of the behavior of the model's separatrix remains an issue for a thorough analysis of the model's parameters and gating variables. This would exceed the scope of this work where our main focus was on the introduction of the separatrix as a more satisfactory 2D threshold concept.

3.3.5 Conclusion

The work at hand has three main aspects:

First, the results presented in this work give strong evidence that a pure voltage threshold is insufficient to analyse properties necessary for spike initiation in sharp intracellular recordings. Taking $\dot{U}$ into account as a second state variable besides U seems to complete the phenomenological state space of neurons in respect to spike initiation. Thus, it seems advisable to use the 2-dimensional state space with the 2-dimensional threshold concept for any analysis work if detailed knowledge about the spike initiation threshold is of central importance.

Second, the algorithm presented in chapter 2 provides a new analysis tool that allows a precise, detailed and robust analysis of the point of neural spike initiation. We have shown the SIPs detected by the algorithm to be very close to the real ones if the spike onset is kinky enough (which is the case for real neurons). Thus, all results give strong evidence that the SIPs found by the algorithm are sufficiently close to the real ones for detailed further analysis.

Third, the separatrix concept developed in chapter 3 promises to be a potent tool to phenomenologically describe the threshold behavior of a neuron. We were able to show that all models as well as all neurons have such a threshold separatrix within the U-$\dot{U}$ state space. We were also able to show that the separatrices found using our algorithms always reproduced the key features - angle, curvature as well as relative range - of the real separatrices of the models analyzed. This is a strong evidence for the correctness of the separatrix concept as well as the reliability of the analysis procedure.

Being a relatively simple toolkit that works simply on recorded voltage traces, the separatrix concept should also allow quick re-analysis of existing as well as new data in order to determine and verify computational, pharmacological, morphological or functional correlations of separatrix types.

We can now answer the questions asked in 1.3:

- We can precisely determine the SIP for a spike using the algorithm presented in chapter 2.
- $\dot{U}$ is a suitable second threshold parameter.
  - Both cells and models do exhibit separatrices
  - The results of this work do not indicate that a 2-D state space would be insufficient
  - There are various forms of separatrices, from horizontal via backslash and vertical to slash-type separatrices.
  - Model separatrices can be found in cells, but not all cell separatrices have been observed in the models.
  - 4-AP does affect the separatrices in the models, but there is no clear effect in the cells.

3.3.6 Outlook

The next step would of course be to analyze the functional consequences of different separatrices. What is the difference between cells with a vertical or a horizontal separatrix? Do they incorporate different network properties? Can cells change their separatrices to adopt to some functional changes? What happens if the procedures presented here are applied to natural spike trains? Will we be able to watch a separatrix shift?

If it turns out that the type of separatrix is a central key element to define neural function this would again challenge the Hodgkin-Huxley models - at least if it turns out that they can only have the slash-type separatrix found in the models tested here. On the other hand this could allow a significant computational simplification when modeling larger neural networks: pre-defined separatrices can easily be incorporated into many simple models like the leaky integrate-and-fire model shown here. Already this model is computationally much simpler than Hodgkin-Huxley models, allowing simulation of large networks with only a fraction of computational power that would be necessary for Hodgkin-Huxley networks. This especially holds as there are a number of enhancements and optimizations that make leaky integrate-and-fire models more and more "physiological", thereby retaining most of their simplicity ([8, 13, 17, 39, 43], see also the work of Burkitt [11, 12] for a review).

Bibliography

[1] F. Awiszus. Reduction of a Hodgkin-Huxley-type model for a mammalian neuron at body temperature. *Biological Cybernetics*, 67:427–432, 1992.

[2] R. Azouz and C. M. Gray. Cellular mechanisms contributing to response variability of cortical neurons in vivo. *J Neurosci*, 19(6):2209–23, 1999.

[3] R. Azouz and C. M. Gray. Dynamic spike threshold reveals a mechanism for synaptic coincidence detection in cortical neurons in vivo. *Proc Natl Acad Sci U S A*, 97(14):8110–5, 2000.

[4] R. Azouz and C. M. Gray. Adaptive coincidence detection and dynamic gain control in visual cortical neurons in vivo. *Neuron*, 37(3):513–23, 2003.

[5] M. V. L. Bennett, B. Hille, and S. Obara. Voltage threshold in excitable cells depends on stimulus form. pages 585–593, 197.

[6] J. Bernstein. *Untersuchungen über den Erregungsvorgang im Nerven- und Muskelsysteme.* Carl Winter's Universitätsbuchhandlung, Heidelberg, 1871. (Investigations on the Activation Process of Nerve and Muscle Systems).

[7] J. Bernstein. Untersuchungen zur Thermodynamik der bioelektrischen Ströme. *Pflügers Archiv*, 92:521–562, 1902. (Investigations on the Thermodynamics of Bio-Electrical Currents).

[8] R. Brette. Exact simulation of integrate-and-fire models with synaptic conductances. *Neural Comput*, 18(8):2004–27, 2006.

[9] D. R. Brillinger and J. P. Segundo. Empirical examination of the threshold model of neuron firing. *Biological Cybernetics*, 35:213–220, 1979.

[10] H. L. Bryant and J. P. Segundo. Spike initiation by transmembrane current: A white-noise analysis. *J. Physiol.*, 260:279–314, 1976.

[11] A. N. Burkitt. A review of the integrate-and-fire neuron model: I. Homogeneous synaptic input. *Biol Cybern*, 95(1):1–19, 2006.

[12] A. N. Burkitt. A review of the integrate-and-fire neuron model: II. Inhomogeneous synaptic input and network properties. *Biol Cybern*, 95(2):97–112, 2006.

[13] B. Cartling. A low-dimensional, time-resolved and adapting model neuron. *Int J Neural Syst*, 7(3):237–46, 1996.

[14] P. Cobbett, P. Legendre, and W. T. Mason. Characterization of three types of potassium current in cultured neurones of rat supraoptic nucleus area. *J Physiol*, 410:443–62, 1989.

[15] P. Cobbett and W. T. Mason. Whole cell voltage clamp recordings from cultured neurons of the supraoptic area of neonatal rat hypothalamus. *Brain Res*, 409(1):175–80, 1987.

[16] C. M. Colbert and D. Johnston. Axonal action-potential initiation and Na+ channel densities in the soma and axon initial segment of subicular pyramidal neurons. *Journal of Neuroscience*, 16(21):6676–6686, 1996.

[17] A Destexhe. Conductance-based integrate-and-fire models. *Neural Comput*, 9(3):503–14, 1997.

[18] C. Ebbinghaus. Charakterisierung der neuronalen Feuerschwelle. Master's thesis, Universität Tübingen, November 1997.

[19] G. B. Ermentrout. Phase-Plane Analysis of Neural Activity. In *The Handbook of Brain Theory and Neural Networks*. MIT Press, 1998. ISBN: 0-262-51102-9.

[20] E. Ficker and U. Heinemann. Slow and fast transient potassium currents in cultured rat hippocampal cells. *J Physiol*, 445:431–55, 1992.

[21] A. Foust, M. Popovic, D. Zecevic, and D. A. McCormick. Action potentials initiate in the axon initial segment and propagate through axon collaterals reliably in cerebellar Purkinje neurons. *J Neurosci*, 30(20):6891–902, 2010.

[22] B. Gutkin and G. B. Ermentrout. Spikes Too Kinky in The Cortex. *Nature*, 440:999–1000, 20 April 2006.

[23] H. L. Haas, B. Schaerer, and M. Vosmansky. A simple perfusion chamber for the study of nervous tissue slices in vitro. *J Neurosci Methods*, 1(4):323–5, 1979.

[24] A. L. Hodgkin and A. F. Huxley. A quantitative description of membrane current and its application to conduction and excitation in nerve. *J Physiol*, 117(4):500–44, 1952.

[25] E. M. Izhikevich. Class 1 neural excitability, conventional synapses, weakly connected networks, and mathematical foundations of pulse-coupled models. *IEEE Trans Neural Netw*, 10(3):499–507, 1999.

[26] E. M. Izhikevich. Neuronal excitability, spiking, and bursting. *International Journal of Bifurcation and Chaos*, 10:1171–1266, 2000.

[27] R. Klee, E. Ficker, and U. Heinemann. Comparison of voltage-dependent potassium currents in rat pyramidal neurons acutely isolated from hippocampal regions CA1 and CA3. *J Neurophysiol*, 74(5):1982–95, 1995.

[28] C. Koch. The Hodgkin-Huxley model of action potential generation. In *The Biophysics of Computation*, chapter 6, page 139 ff. Oxford University Press, 1999.

[29] L. Lapicque. Recherches quantitatives sur l'excitation électrique des nerfs traitée comme une polarization. *J. Physiol. Pathol. Gen.*, 9:620–635, 1907. Leaky Integrate-And-Fire-Neuron.

[30] K. Lucas. On the rate of variation of the exciting current as a factor in electric excitation. *J. Physiol.*, 36:253–274, 1907.

[31] Z. F. Mainen, J. Joerges, J. R. Huguenard, and T. J. Sejnowski. A model for spike initiation in neocortical pyramidal neurons. *Neuron*, 15(6):1427–1439, 1995.

[32] M. Martina, I. Vida, and P. Jonas. Distal initiation and active propagation of action potentials in interneuron dendrites. *Science*, 287:295–300, 2000.

[33] D. A. McCormick, Y. Shu, and Y. Yu. Hodgkin And Huxley Model - Still Standing? *Nature*, 445(10.1038/nature05523):E1–E2, 2007.

[34] R. Melinek and K. J. Muller. Action potential initiation site depends in neuronal excitation. *Journal of neuroscience*, 16:2585–2591, 1996.

[35] W. Muller, U. Misgeld, and U. Heinemann. Carbachol effects on hippocampal neurons in vitro: dependence on the rate of rise of carbachol tissue concentration. *Exp Brain Res*, 72(2):287–98, 1988.

[36] B. Naundorf, F. Wolf, and M. Volgushev. Unique Features of Action Potential Initiation in Cortical Neurons. *Nature*, 440:1060–1063, 20 April 2006.

[37] B. Naundorf, F. Wolf, and M. Volgushev. Naundorf et al. Reply. *Nature*, 445(10.1038/nature05534):E2–E3, 2007.

[38] H. Querfurth. Action-potential initiation and maintained activity of the isolated frog muscle spindle. *Eur J Neurosci*, 24(4):1147–56, 2006.

[39] M. J. Shelley and L. Tao. Efficient and accurate time-stepping schemes for integrate-and-fire neuronal networks. *J Comput Neurosci*, 11(2):111–9, 2001.

[40] G. Y. Shen, W. R. Chen, J. Midtgaard, G. M. Shepherd, and M. L. Hines. Computational analysis of action potential initiation in mitral cell soma and dendrites based on dual patch recordings. *J. Neurophysiol.*, 82:3006–3020, 1999.

[41] P. M. Sonner and J. E. Stern. Functional role of A-type potassium currents in rat presympathetic PVN neurones. *J Physiol*, 582(Pt 3):1219–38, 2007.

[42] G. Stuart, N. Spruston, B. Sakmann, and M. Häusser. Action potential initiation and backpropagation in neurons of the mammalian CNS. *Trends in Neuroscience*, 20(3):125–131, 1997.

[43] A. Tonnelier, H. Belmabrouk, and D. Martinez. Event-driven simulations of nonlinear integrate-and-fire neurons. *Neural Comput*, 19(12):3226–38, 2007.

[44] A. A. Verveen. On the fluctuation of threshold in nerve fibre, 1960.

[45] X.-J. Wang and G. Buzsáki. Gamma oscillation by synaptic inhibition in a hippocampal interneuronal network model. *Journal of Neuroscience*, 16(20):6402–6413, 15 October 1996.

[46] Y. Yu, Y. Shu, and D. A. McCormick. Cortical action potential backpropagation explains spike threshold variability and rapid-onset kinetics. *J Neurosci*, 28(29):7260–72, 2008.

Appendix A

Supplements

A.1 Abstract

It is generally accepted that neural spikes are initiated solely by a voltage threshold mechanism. However, when looking at intracellular voltage recordings, the voltage U exhibits a significant range of voltage values, thus contradicting the threshold concept as such.

From a dynamical systems perspective one clearly would conclude therefrom that the system is insufficiently described using U alone as a state variable. Inspired by qualitative reports of neurons that can be driven far beyond their (voltage) threshold when stimulating them slowly enough, we introduced the first time derivative of the voltage, $\dot{U}$, as a second state variable. Plotting spikes within this two-dimensional state space suggests that they can be locally interpreted as a dynamical system with two attractors: one being the resting potential, the other one being the spike voltage maximum (due to the the Na equilibrium potential). These two attractors can be imagined to be separated by a boundary line, a so-called separatrix. This separatrix would thus be composed of points at which a spike has become unavoidably.

In order to verify the separatrix as a 2D firing threshold in U and $\dot{U}$ these spike initiation points have to be identified as precise as possible. In physiological data the spike is characterized by a sharp kink at spike onset where it abruptly and vertically emerges from the sub-threshold activity. An algorithm has been developed that - both starting from the sub-threshold as well as from the super-threshold domain - is able to identify these points reliably, precise and robustly.

This procedure was verified using Hodgkin-Huxley type and leaky integrate-and-fire models. Here the real spike initiation points could be determined by

successively shortening stimulus length. During analysis it turned out that most Hodgkin-Huxley type models show a very shallow spike onset which in in clear contrast to the sharp onset in cells. We could show that the found spike initiation points are the more distant from the real ones the shallower the spike onset was. On the other hand, if the model showed an abrupt and vertical spike onset real and found spike initiation points were very close together. Because real neurons show an abrupt and vertical spike onset we can thus expect the detected spike initiation points to be identical to the real ones.

Both cells and models were then stimulated with ramps of different slopes in order to test the threshold dependence on $\dot{U}$. The new algorithm was then used to detect the spike initiation points for the first spike of each ramp. A curve was fitted to these points within the U-$\dot{U}$ state space, thus resembling the separatrix of the cell.

We could show that all cells exhibit a separatrix. All 4 possible orientation classes were found: vertical (i.e. a pure voltage threshold), horizontal (i.e. a pure $\dot{U}$ threshold), slash-type (i.e. from lower left to upper right) and backslash-type (i.e. from lower right to upper left). Hodgkin-Huxley type models showed mainly slash-type separatrices and a vertical one in one case. Leaky integrate-and-fire models with predefined separatrices were used for verification, and the algorithm was able to reproduce all of these predefined separatrices.

The neural separatrices showed temporal stability (when cellular state parameters were constant) and independence of positive or negative offset. On the other hand, small changes in cell parameters (membrane time constant, resistance, resting potential) showed clear changes and shifts in the separatrices, thus indicating at them to be a highly sensible indicator of cell state. Pharmacological experiments with A-type channel blockers did not exhibit a systematical effect as - due to the sensitivity addressed above - already the necessary block cocktail changes cell parameters, thus shifting the separatrix.

A.2 Zusammenfassung

Es ist ein allgemein anerkanntes Kozept, dass neuronale Aktionspotenziale mittels eines einfachen Schwellenmechanismus der Membranspannung U induziert werden. Schaut man sich jedoch die Initiationspunkte von Spikes innerhalb einer Zelle genauer an, so wird eine bemerkenswerte Variabilität der Spannungswerte zu Spikebeginn deutlich, was dem Modell einer Spannungsschwelle jedoch widerspricht.

Aus Sicht der mathematischen Konzepte der dynamischen Systeme ist ein solches Phänomen ein Zeichen für einen unterdimensionierten Zustandsraum, in dem (mindestens) eine Zustandsvariable fehlt. Inspiriert durch die immer wieder kolportierten Phänomene, dass Zellen ohne Spike deutlich über ihre Spannungsschwelle depolarisiert werden können, wenn dies nur langsam genug geschieht, wurde die erste Ableitung der Spannung nach der Zeit, $\dot{U}$, als zweite Zustandsvariable eingeführt. Die Darstellung von Spikes in diesem Zustandsraum legt nahe, dass man sie vorübergehend als dynamisches System auffassen kann, in dem sich zwei Attraktoren - das Ruhepotential auf der einen Seite, das Spikemaximum (bedingt durch das Na-Gleichgewichtspotenzial) auf der anderen Seite - befinden, die durch eine Separatrix, eine Grenzlinie voneinander getrennt sind. Diese Separatrix müsste demnach aus den Punkten bestehen, an denen im neuronalen Zustandsraum ein Spike unwiderruflich initiiert wurde.

Für die Verifikation der Separatrix als einer 2-dimensionalen Feuerschwelle aus U und $\dot{U}$ müssen diese Punkte der Spikeentstehung möglichst präzise bestimmt werden. Phänomenologisch sind sie in den Daten durch einen scharfen Knick gekennzeichnet, in dem der Spikeansatz sich aprupt nahezu senkrecht aus der unterschwelligen Aktivität erhebt. Es wurde ein Algorithmus entwickelt, der sowohl ausgehend von der unterschweligen als auch von der überschwelligen Domäne diesen Spikeinitiationspunkt zuverlässig, präzise und robust finden kann.

Dieses Verfahren wurde an Modellen verifiziert, in denen zusätzlich die echten Spikeinitiationspunkte durch sukzessive Stimulusverkürzung bestimmt wurden. Dabei wurde deutlich, das die meisten Hodgkin-Huxley-Modelle im Gegensatz zu Zellen einen unphysiologisch flachen Spikebeginn besitzen. Während bei Modellen mit schnellem Spikebeginn der gefundene Spikeinitiationspunkt gut mit dem echten übereinstimmt, wird er bei den anderen um so später detektiert, je flacher der Spike beginnt. Da die gemessenen Zellen alle über einen aprupten Spikebeginn verfügen, kann davon ausgegangen werden, dass der Algorithmus die Spikeinitiationspunkte präzise detektiert.

Zellen und Modelle wurden nun mit verschieden steilen Rampen stimuliert, um die Abhängigkeit der Schwelle von $\dot{U}$ zu testen. Für die so

induzierten Spikes wurden nun mittels des beschriebenen Algorithmus die Spikeinitiationspunkte bestimmt. An die so gefundenen Punkte wurde im U-$\dot{U}$-Zustandsraum eine Funktion gefittet, die die Separatrix für die jeweilige Zelle bzw. das jeweilige Modell darstellt.

Es konnte gezeigt werden, dass alle Zellen eine Separatrix besitzen. Es sind alle wurden alle Orientierungen beobachtet: senkrecht (entsprechend einer reinen Spannungsschwelle), waagerecht (entsprechend einer reinen $\dot{U}$-Schwelle) sowie ihre Kombinationen (schräg von links unten nach rechts oben (slash-Typ) als auch von links oben nach rechts unten (backslash-Typ)). Hodgkin-Huxley-Modelle zeigten nur eine slash-Typ-Separatrix sowie in einem Fall eine senkrechte. Für Testzwecke wurden spikende Leaky Integrate-and-Fire-Modelle mit vordefinierten Schwellseparatrices eingesetzt, die von den vorgestellten Algorithmen präzise reproduziert werden konnten.

Die Separatrices bei den Zellen zeitlich stabil (bei gleichbleibenden Zellparametern) und unabhängig von einem positiven oder negativen Offset. Andererseits zeigten sich bereits bei kleinen Änderungen der Zellparameter deutliche Änderungen in der Separatrix, was auf eine hohe Sensibilität der Separatrices für den Zellzustand hinweist. Pharmakologische Experimente mit A-Kanal-Blockern zeigten keinen systematischen Effekt, da bereits die Gabe des zur Vermeidung epileptiformer Aktivitäten notwendige Block-Cocktail die Separatrix veränderte, bevor der A-Kanal-Block zugegeben wurde.

A.3 Acknowledgements

Many people have contributed to this work in a variety of ways. I would like to thank them here, those named below, but also those who I forgot to mention.

Andreas Herz gave me the opportunity to pursue these ideas in his Lab. Jan Benda, Daniel Cremers and Martin Stemmler were always available and willing to discuss and criticize approaches and concepts. Laurenz Wiskott helped me to focus thoughts. Petra Prinz and Daniela Efler also discussed ideas and concepts, provided data and especially helped in going through motivational lows.

Uwe Heineman supported the experiments both practically as well as theoretically. His experience was extremely valuable to overcome the pits of practical electrophysiology and interpret cellular responses. He also never stopped to support the finishing of this dissertation. Andreas Draguhn and Dietmar Schmitz supported the work with discussions and hints. The experiments were done together with Gunter Kreck with whom I took the first electrophysiological steps together.

Jan Benda, Daniel Cremers and Andreas Draguhn kindly offered their time to thoroughly discuss the first versions of this dissertation. They made valuable remarks and supported me in finishing the work.

Randolf Menzel was immediately supportive when in need of a supervisor. He was interested in the work and supported my attempt to finish it. I thank him very much for being available any time and for his pragmatic calmness. Martin Nawrot was so kind to supervise the last steps of the work. He gave valuable hints on argumentation and structure.

Most of all, however, I would like to thank my friend, partner and wife Silke Erdmann for her patience as well as her impatience. She supported me during the lows and corrected me during phases of ignorance. I owe her a lot. And last but not least I would like to thank my daughter Lena Erdmann for her patience and for (mostly) silently accepting that her father could not go swimming because of his dissertation.

Contact

For further questions you may contact the author at **carsten** *dot* **erdmann** *at* **email** *dot* **de**.